Development of the large GEM tracker and the trigger system for the J-PARC E16 experiment

Yuki Obara
The University of Tokyo

October 1, 2015

Abstract

In the J-PARC E16 experiment, mass spectra of light vector mesons in nuclear matter are measured with high precision and high statistics to investigate a restoration of the chiral symmetry at a normal nuclear density.

For the E16 experiment, a new spectrometer which has high rate capability for high intensity beam at J-PARC and a good mass resolution is need to be constructed. A GEM tracker is used for tracking charged particles. The GEM tracker is required to have a good spatial resolution better than 100 μm for an incident angle from 0° to 30°. A $300 \times 300\,\mathrm{mm}^2$ GEM tracker needs to generate a trigger signal from the last GEM foil. The large GEM tracker was developed to fulfill the requirements.

For the trigger system, a new GEM foil which has 24 electrodes and a new dedicated ASIC are developed and their performance are evaluated. As a result, the new developed large GEM has gain of 10^4 which enough to achieve a good spatial resolution and high trigger efficiency, and the new ASIC can successfully pick a trigger signal from GEM foil.

The position resolution and detection efficiency of the large GEM trackers are evaluated by a beam test. The obtained position resolution is better than 100 μm for the incident angle from 0° to 30°. As a conclusion, we are ready to start a final detector production for the GEM tracker.

Contents

Chapter 1

Introduction

The strong interaction of quarks and gluons is well described by quantum chromodynamics (QCD), which is a non-Abelian gauge theory with the color gauge group $SU(3)$. The Lagrangian density of QCD $\mathcal{L}_{\rm QCD}$ is

$$\mathcal{L}_{\rm QCD} = \sum_q (\bar{q}_L i \not{D} q_L + \bar{q}_R i \not{D} q_R) - \frac{1}{4} G^a_{\mu\nu} G^{a\mu\nu} - \sum_q (\bar{q}_L m q_R + \bar{q}_R m q_L) \tag{1.1}$$

where q are three light flavors (u, d, s) and m is mass matrix $\mathrm{diag}(m_u, m_d, m_s)$.

One of the most important feature of QCD is the running coupling constant $\alpha_s(Q^2)$ which is defined as an effective coupling strength among quarks and gluons at energy scale or momentum transfer Q. The coupling constant satisfies the renormalization group equation

$$Q^2 \frac{d\alpha_s}{dQ^2} = \beta(\alpha_s) = -(b_0 \alpha_s^2 + b_1 \alpha_s^3 + \cdots) \tag{1.2}$$

where $b_0 = (33 - 2n_f)/12\pi$ (1-loop) and $b_1 = (153 - 19n_f)/24\pi^2$ (2-loop) are the β-function coefficients, and n_f is the number of flavors. Due to the minus in Eq. (1.2), the coupling constant $\alpha_s(Q^2)$ becomes small as Q increases, which is called asymptotic freedom of QCD [1]. The running coupling constant $\alpha_s(Q^2)$ is a simple analytic solution for Eq. (1.2) and in the two-loop perturbation theory it is given by

$$\alpha_s(Q^2) = \frac{1}{b_0 \ln(Q^2/\Lambda^2)} \left(1 - \frac{b_1}{b_0^2} \frac{\ln(\ln(Q^2/\Lambda^2))}{\ln(Q^2/\Lambda^2)} \right) \tag{1.3}$$

where Λ is called the QCD scale parameter ($\sim 200\,\mathrm{MeV}$). At high energy region, perturbative methods are successfully used to calculate physical quantity. Eq. (1.3) and Figure 1.1 demonstrates that the running coupling constant α_s increases and becomes strong at low energies $Q \sim \Lambda$. In this energy scale, perturbative calculations can not be applied and, various nonperturbative effects such as the confinement [3] and breaking of the chiral symmetry [4, 5] occur.

Quarks acquire their current mass ($m_u, m_d \simeq$ a few $\mathrm{MeV}/c^2, m_s \simeq 100\mathrm{MeV}/c^2$) through the Higgs mechanism. Mass of constituent quark in hadrons and nuclei is caused by the spontaneous breaking of the chiral symmetry which plays an essential role in QCD at low energy. Therefore, quantitative understanding of QCD in low energy scale is necessary in order to investigate the origin of hadron mass.

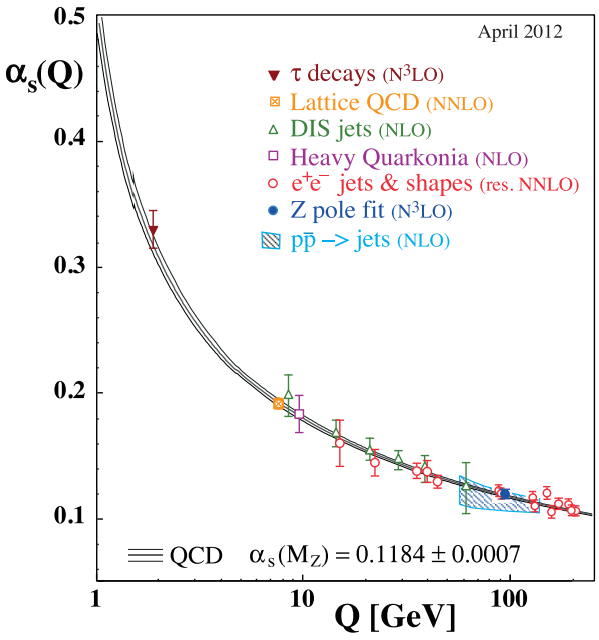

Figure 1.1: Summary of measurements of α_s as a function of the energy scale Q [2].

The QCD Lagrangian is invariant under the chiral transformation ($q \to e^{-i\gamma_5\theta}q$) in massless limit ($m_u, m_d, m_s \to 0$). When the spontaneous breaking of the chiral symmetry occurs, quark-antiquark pairs condense in the vacuum and, constituent quarks in hadrons interact with the condensate and gain their effective mass. Quark condensate $\langle\bar{q}q\rangle$ is an order parameter of the chiral symmetry. The order parameter $\langle\bar{q}q\rangle$ becomes zero with the chiral symmetric phase, while it becomes finite value with the chiral symmetry broken phase.

Temperature and density dependence of the quark condensate $\langle\bar{q}q\rangle$ is illustrated with Fig. 1.2. As temperature (density) increases, absolute value of $\langle\bar{q}q\rangle$ decreases and finally goes to zero at the critical temperature (density). In hot (finite temperature) and/or dense (finite density) matter, chiral phase transition takes place and the spontaneous breaking chiral symmetry is restored. Unfortunately, $\langle\bar{q}q\rangle$ itself is not an observable, therefore other observables such as spectral properties of hadrons like mass and decay width which reflect the value of $\langle\bar{q}q\rangle$ should be used. In other words, measurements of hadron properties in hot/dense matter are powerful tools to search the chiral symmetry restoration in the matter.

There are several theoretical approaches to the hadron properties in the medium [7, 8, 9, 10, 11]. In particular, QCD sum rule shows that a mass spectrum in the medium has to change as a result of the chiral symmetry restoration. Hatsuda and Lee studied using the QCD sum rule and calculated density dependence of light vector mesons (ρ, ω, ϕ) [8]. They predicted 10∼20% decreasing for ρ, ω and 2∼4% for ϕ at normal nuclear density ($\rho_{\rm nucl} \sim 0.17\,{\rm fm}^{-3}$) as shown in Fig. 1.3.

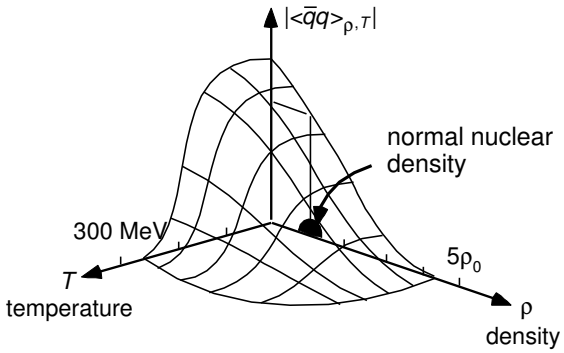

Figure 1.2: Quark condensate $|\langle\bar{q}q\rangle|$ as a function of temperature T and density ρ [6].

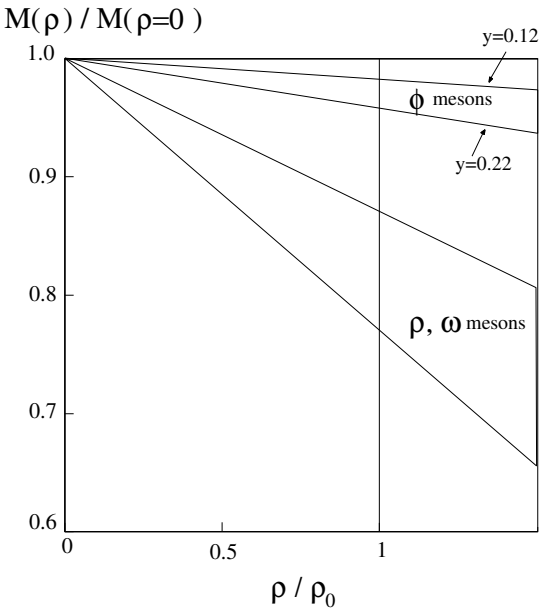

Figure 1.3: Mass modification of vector mesons in finite density predicted by Hatsuda and Lee [8].

Several experiments already detected the modification of light vector mesons spectra in hot/dense matter. For examples, the CERES experiment at CREN-SPS [12], the NA60 experiment also at CREN-SPS [13], the KEK-PS E325 experiment [14, 15], the CLAS-g7 at JLab [16], the CBELSA/TAPS experiment [17] and the LEPS at Spring-8 [18]. Heavy ion collision or nuclear reaction can generate a hot/dense medium and, the in-medium mass spectrum of light vector mesons is reconstructed from their decay products. From the viewpoint of measuring the decay products, lepton pair decays are suitable, since there is no final state interaction between leptons and the medium. All the experiments agree that mass spectra of the light vector mesons are modified in hot/dense medium. However, details of the

modifications are different. Especially, only the KEK-PS E325 experiment states a mass shift of the vector mesons. The result of the KEK-PS E325 which is the predecessor experiment of the J-PARC E16 experiment is reviewed below.

The experiment KEK-PS E325 was carried out at the EP1-B primary beam line at KEK 12 GeV Proton Synchrotron. Invariant mass spectra of e^+e^- pairs produced in a nuclear reaction $\mathrm{p} + \mathrm{A} \to \rho/\omega/\phi$ was investigated. The spectrometer was designed to detect relatively slowly-moving vector mesons, since such mesons are expected to spend longer time in nuclei after they are produced and to have larger probability of decay inside nuclear matter. In order to search nuclear size dependence of the mass spectra, two types of target, carbon and copper, were used.

The mass spectra with different $\beta\gamma$ range for C and Cu target are fitted with resonance shape of $\phi \to e^+e^-$ and a quadratic background as shown in Fig. 1.4. The C and Cu data with $\beta\gamma > 1.25$ are well reproduced by the fit, while the Cu data with $\beta\gamma < 1.25$ has significant excess on low mass side of the peak of ϕ. Assuming density dependence of ϕ meson mass as $m(\rho)/m(0) = 1 - k_1(\rho/\rho_0)$, where ρ_0 is normal nuclear density, the shift parameter $k_1 = 0.034^{+0.006}_{-0.007}$ is obtained.

The mass spectrum of wider range for C and Cu target is shown in Fig. 1.5. The combinatorial background evaluated by the event-mixing method and the shapes of $\eta \to e^+e^-\gamma$ and $\omega \to e^+e^-\pi^0$ are already subtracted. As the ϕ meson case, supposing that density dependence of ρ and ω meson mass as $m(\rho)/m(0) = 1 - k_1(\rho/\rho_0)$ is estimated to be $\sim 0.092 \pm 0.002$.

The next experiment should confirm the modifications of mass spectra for light vector mesons. In addition, direct measurements of mass spectra in nucleus are very important, since the mass spectra in finite density have strong relation to the amount of quark condensates. In KEK-E325, a combined mass spectra of modified and not-modified was measured due to a limited statistics. Thus, a new experiment is proposed and being prepared at J-PARC.

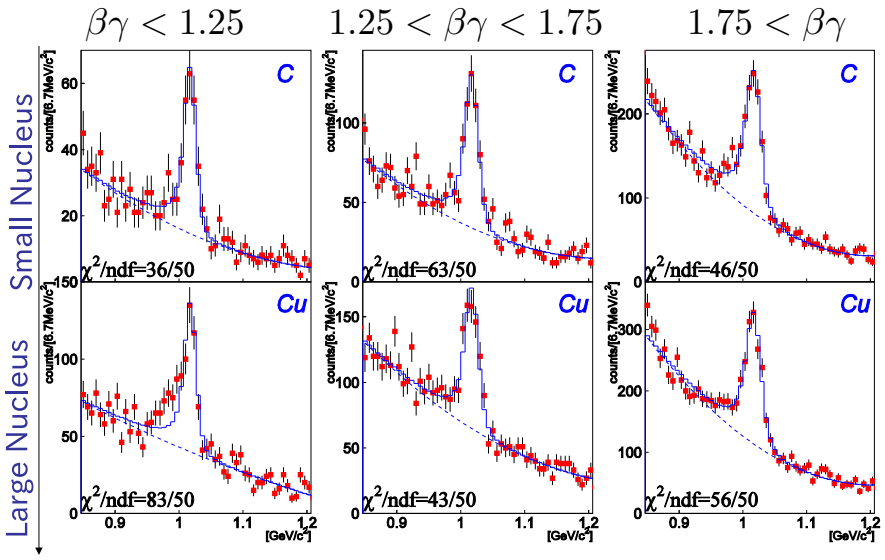

Figure 1.4: A result from E325. Invariant mass spectra of $\phi \to e^+e^-$ in medium. The significant excess on low mass side of ϕ is observed for slowly-moving ϕ in Cu target [14].

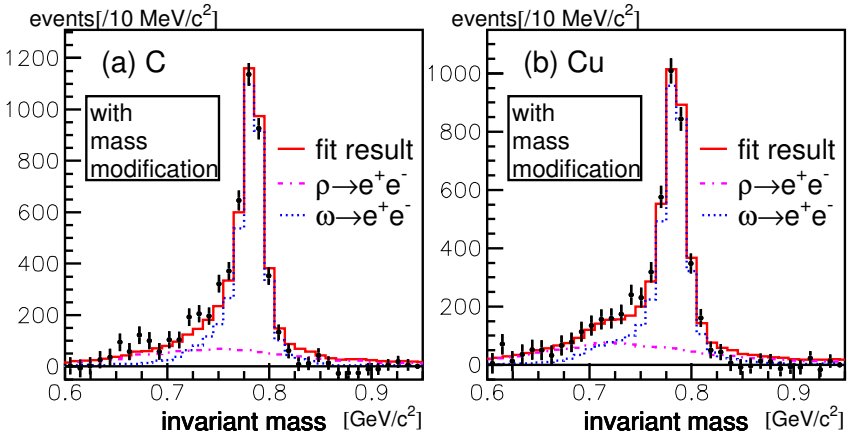

Figure 1.5: A result from E325. Model-fitting result of the invariant mass of $\rho/\omega \to e^+e^-$ in medium [15].

Chapter 2

J-PARC E16 experiment

2.1 Overview

In the J-PARC E16 experiment, we unambiguously measure mass spectra of light mesons in nuclear matter with high precision and high statistics to investigate a restoration of the chiral symmetry at normal nuclear density and origin of hadron mass.

In the E16 experiment, light vector mesons are generated by a nuclear reaction of the 30 GeV proton beam and target nuclei. The mass spectra are reconstructed by e^+e^- pair decay channel which has a small branching ratio, however, does not suffer from final state interaction with the nucleus.

The high intensity proton beam at J-PARC improves statistics by two orders of magnitude compared to the KEK-PS E325 experiment. The improvement of statistics enables us to use new various targets as summarized in Table 2.1. Slowly moving mesons have large probability of their decaying in the target nuclei. Heavy target and proton target are important. Measurement of large nuclei target and proton target was given up in the KEK-PS E325 because of the statistical limitation. An expected spectrum of ϕ meson is shown in Fig. 2.1.

The statistics is expected to be improved from KEK-PS E325 by the following ways.

1. 10 times higher beam intensity
2. 2 times larger cross section
3. 5 times larger acceptance

To achieve the first and the second things, a new beam line at J-PARC is required. The third factor is realized by constructing a new spectrometer.

Another key to measure mass spectra clearly is a good mass resolution for electron pairs. It enables to distinguish a slight tail of modified meson mass spectrum form the background. Effect of experimental invariant mass resolution on the modified ϕ meson mass distribution is shown in Fig. 2.2. The result shows that at

Table 2.1: Targets spec of E325 and E16

	nuclei	thickness (μm)	interaction length (%)	radiation length (%)
E325	C	810	0.21	0.43
	Cu	81	0.054	0.57
E16	C	200	0.05	0.1
	CH_2	400	0.05	0.1
	Cu	80	0.05	0.5
	Pb	20	0.01	0.3

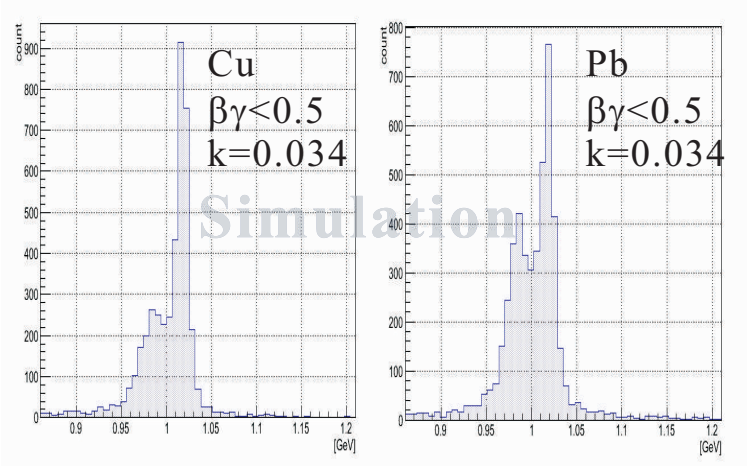

Figure 2.1: Expected spectra in J-PARC E16 experiment.

least approximately 10 MeV in r.m.s. at the ϕ mass, the same level as in KEK-PS E325, must be achieved in the J-PARC E16 experiment. In E16 experiment, a new spectrometer which has high rate capability for high intensity beam at J-PARC and a good mass resolution is need to be constructed.

2.2 Spectrometer design

The spectrometer is designed using following basic concepts.

- Use thin targets ($\sim 0.1\%$ interaction length) in order to suppress a radiation tail in the mass spectra.
- Cope with high interaction rate ($\sim$ 10MHz). Beam intensity of high-momentum beam line is 10^{10} per spill to deal with the thin target and small branching ratio ($\sim 10^{-4}$).
- Large acceptance covering the backward region in CM system to detect slowly moving mesons which have high probability of decaying inside nuclei.
- Achieve $5\,\mathrm{MeV}/c^2$ of a mass resolution.

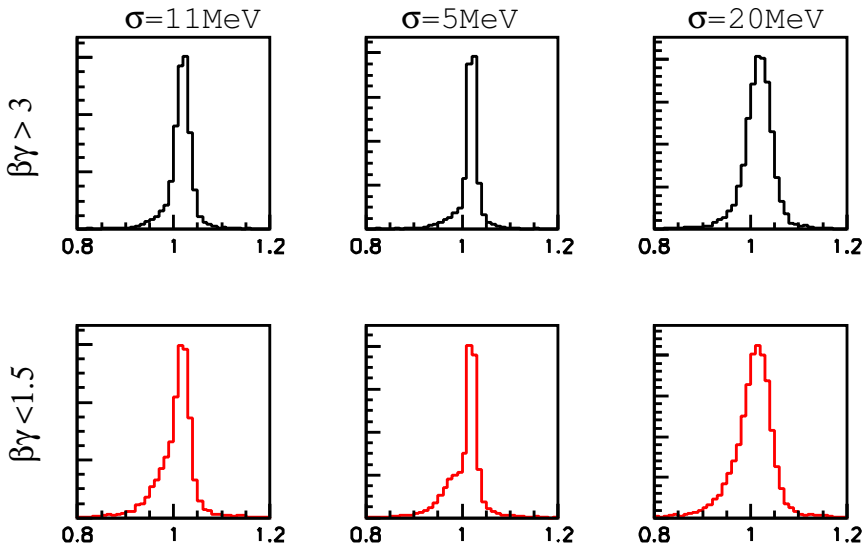

Figure 2.2: The expected modified invariant mass distributions of $\phi \to e^+e^-$ from Cu target with different experimental mass resolution. Upper: fast moving mesons. Lower: slowly moving mesons.

Table 2.2: List of detectors

Detector	Radius (mm)
GEM Tracker 1	200
GEM Tracker 2	400
GEM Tracker 3	600
Hadron Blind Detector	600 - 1100
Lead Glass Calorimeter	1140 - 1700

The new spectrometer has large geometrical acceptance. The acceptance is $\pm 135°$ in horizontal and $\pm 45°$ in vertical except the very forward region of $0° \sim \pm 12°$ both horizontally and vertically to avoid beam halo. Figure 2.3 shows Hadron hall in J-PARC where the spectrometer will be installed. Schematic view of the spectrometer is shown in Fig. 2.4 and Fig. 2.5. The spectrometer consists of tracking detectors and electron identification detectors as follows and a list of the detectors is shown in Table 2.2. These detectors are almost based on Gas Electron Multiplier (GEM)[19].

Target

In a large nucleus such as Pb, possibility of vector meson's decaying is enhanced, which is of critical importance for measurement of mass spectrum in nuclear matter. A radiation length increases rapidly as a nucleus is larger, hence thin target is required for measurement of a large nucleus to reduce a radiation tail. On the other hand, a mass spectrum in proton-on-proton collisions is also very important since

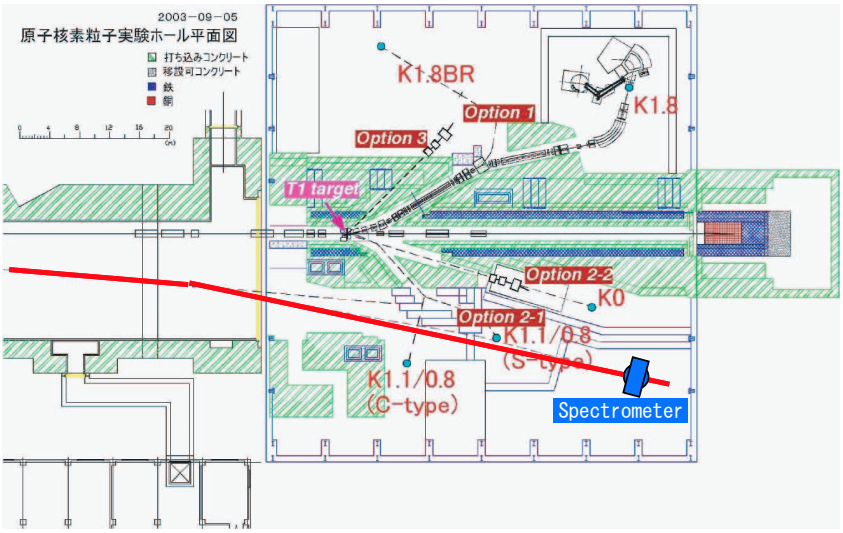

Figure 2.3: Hadron hall in J-PARC and spectrometer

the proton data can be used to subtract a non-modified mass spectrum peak in the spectrum of heavier target nuclei. The mass spectrum of proton target can be obtained by subtracting contribution of a carbon nuclei target from hydrocarbon target data. These features are new at J-PARC, KEK-E325 does not achieve these features due to a statistical limitation.

GEM Tracker

GEM tracker is a micro-pattern gas detector using GEM foils. It was originally developed at the COMPASS experiment [20] for high rate environment and works up to 25kHz/mm^2. In the J-PARC E16 experiment, an expected highest counting rate is 5kHz/mm^2, so this tracking detector is suitable from the viewpoint of coping with high rate counting.

Momenta of electrons and positrons are mainly measured by three layers of GEM tracker in a magnetic field. Their track is determined by vertex information and three hit positions on the tracker and the momentum of them is reconstructed from the tracks. For the momentum region of interest, a required spatial resolution is 100 μm horizontally and 700 μm vertically, which corresponds to a mass resolution of $\sim$ 5 MeV/c^2. An incident angle of up to 30° should be covered. This master thesis focuses on development of this detector. Performance of the GEM tracker and fundamental information about the GEM tracker are described in the following chapter.

Hadron Blind Detector

To acquire pure samples of electron pair, a detector which has high electron identification capability is needed. In E16 experiment, a Hadron Blind Detector (HBD), which was originally developed in the PHENIX experiment, is used as a Čerenkov

counter for electron identification. In the momentum region of electron pair from light vector meson decays, a hadron rejection factor is required to be 100 with an electron detection efficiency of 70% in offline analysis.

Lead Glass Calorimeter

Lead Glass Calorimeter (LG) is a EM calorimeter. In E16 experiment, it is used for electron identification and needs to have a hadron rejection factor of 25. Combination of the HBD and the LG achieves sufficient electron ID capability.

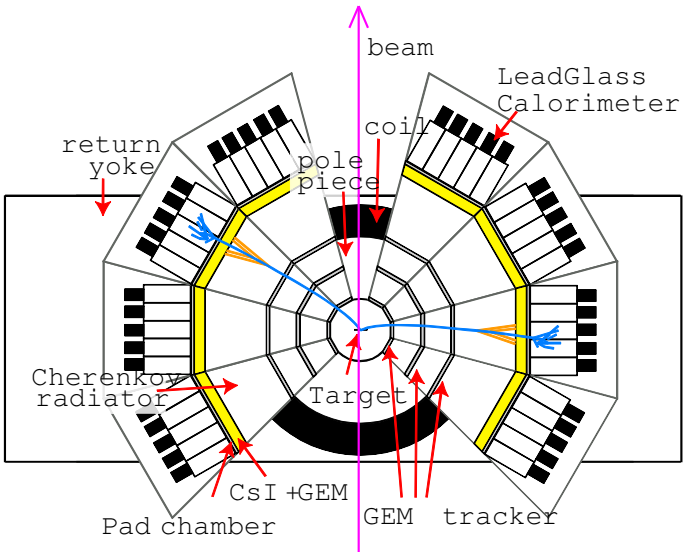

Figure 2.4: A schematic view of spectrometer

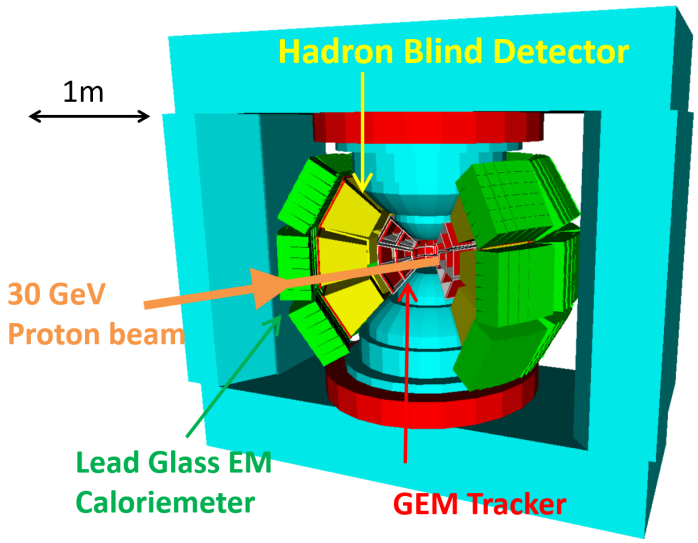

Figure 2.5: A schematic view of spectrometer

Chapter 3

GEM tracker

3.1 Configuration of GEM tracker

A schematic view and a photograph of a GEM tracker are shown in Fig. 3.1 and Fig. 3.2, respectively. The tracker consists of a drift cathode plane (mesh) made of aluminized Mylar, a triple GEM foils stack, and a two-dimensional readout board.

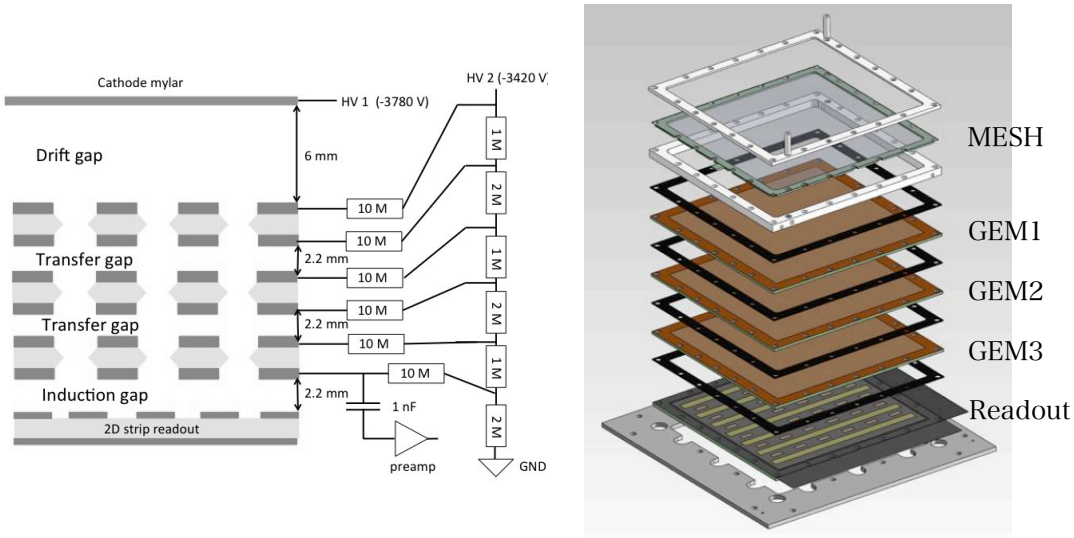

Figure 3.1: A schematic of GEM tracker

3.1.1 Gas Electron Multiplier

Gas Electron Multiplier (GEM) is a thin insulator which is sandwiched by two thin copper layers and has many of small holes as shown in Fig. 3.3. GEM is a kind of micro pattern gas detectors (MPGDs) and originally invented at CERN. Typical thickness of the insulating foil and the electrodes of copper is $50\,\mu$m and $4 \sim 5\,\mu$m, respectively. Size of holes is typically $65\,\mu$m and hole pitch is $140\,\mu$m. GEM is operated by applying suitable high voltage between the electrodes in amplification gas. In the holes, a strong electric filed is formed by high voltage and ionized electrons are amplified by electron avalanche.

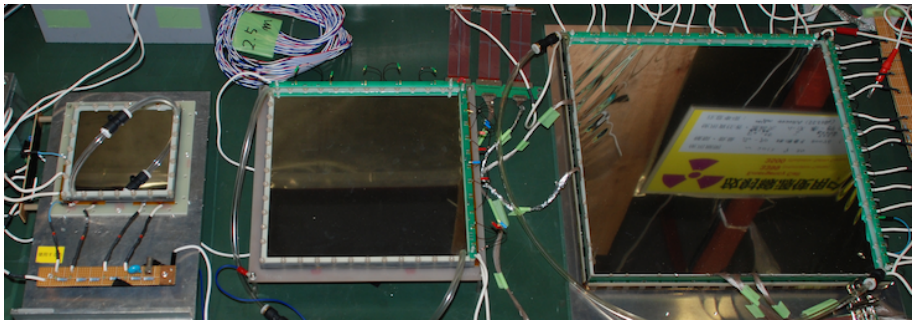

Figure 3.2: A photograph of GEM trackers

Advantages of GEM detectors are following.

1. High gain ($\sim 10^4$) can be achieved by using three layers of GEM foils.
2. GEM has a high rate capability because of the fine hole pitch.
3. An amplification region and a readout board can be separated. It enables us to use perpendicular strip readout board to obtain two-dimensional information of a hit position.

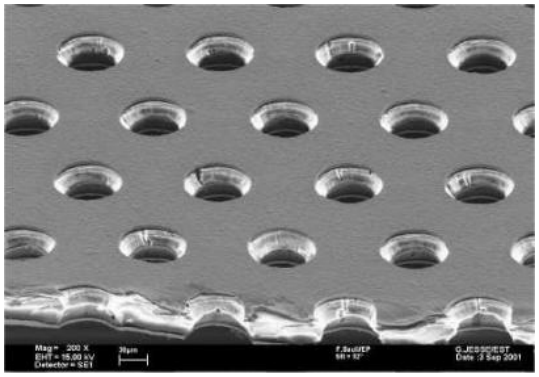

Figure 3.3: View of typical GEM foil[21]

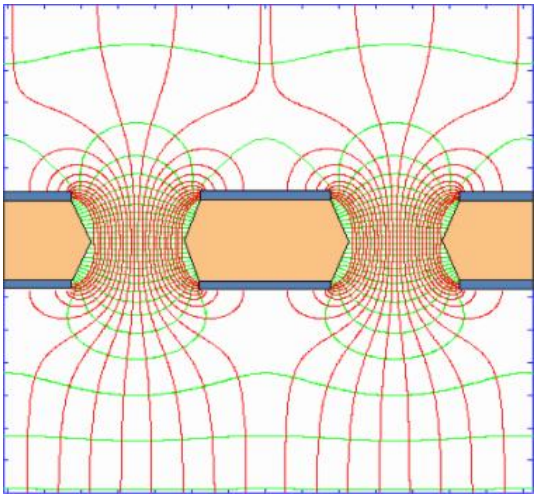

Figure 3.4: View of a electric filed in holes[21]

In our configuration, three GEM foils are stacked in a chamber and a mixture of Ar (70%) and CO_2 (30%) is used for amplification gas. The design of a GEM foil is summarized in Table 3.1.

A GEM is manufactured by a wet etching method. Copper and polyimide (PI) are etched by chemicals to make holes. Figure 3.5 shows a typical hole shape of a $100 \times 100\,\mathrm{mm}^2$ GEM. The copper layer of a large GEM are divided into several segments to reduce capacitance and damage by discharge. The size of $200 \times 200\,\mathrm{mm}^2$ GEM is divided into 4 segments on one side and that of $300 \times 300\,\mathrm{mm}^2$ GEM is

Table 3.1: Design of GEM foil

size (mm)	thickness (μm)	metal (Cu) diameter (μm)	hole (PI) diameter (μm)	hole pitch (μm)
100	50	65	35	140
200	50	65	25	140
300 (12-div)	50	65	25	140
300 (24-div)	50	55	25	140

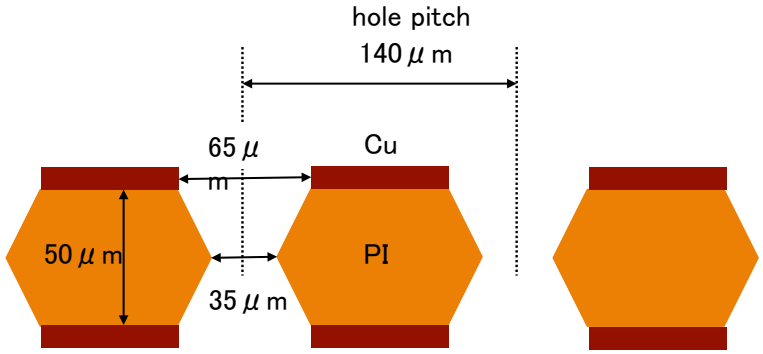

Figure 3.5: Typical hole shape of $100 \times 100\,\mathrm{mm}^2$ GEM.

divided into 12 segments on one side. The bottom GEM is divided into 24 segments on both sides for the GEM foil trigger. As the holes are smaller, the higher relative gain is obtained. We optimized the size of the hole of Cu and PI.

The large acceptance and low material budget are important in the E16 experiment to measure the spectra with high statistics and low background. The GEM tracker seals the amplification gas by a frame of GEM foil to obtain the large acceptance. Width of the frame is narrow and, a material budget of that is low in order to decrease a total material budget of the tracker.

3.1.2 Readout

A readout board has Cartesian strips called "X" and "Y". For a $100 \times 100\,\mathrm{mm}^2$ and $200 \times 200\,\mathrm{mm}^2$ GEM tracker, the readout board are patterned on the top and the bottom side of the polyimide sheet respectively. A photograph of the readout board is shown in Fig. 3.6. The polyimide sheet has a thickness of $25\,\mu$m and the strip pattern is made of copper with a thickness of $4\,\mu$m. The X strips are covered with a $2\,\mu$m nickel plating to prevent an electrical breakdown in the strip pattern. The electrodes seem white due to the plated nickel. It has island electrodes with blind-via-hole (BVH) to transport the charge from the top side islands to the bottom side Y-strips and share the charge between the X and Y strips. The values of strip pitch and width are summarized in Table 3.2. Figure 3.7 shows a $200 \times 200\,\mathrm{mm}^2$ readout board.

A single-side readout board is used for a $300 \times 300\,\mathrm{mm}^2$ GEM tracker as shown in Fig. 3.8. The readout board also has X and Y strips. The readout strips are

manufactured on both sides of polyimide foil which has 25 μmm thickness. The polyimide above Y-strips is removed, and hence both X and Y strips can be directly seen from the top side. The values of strip pitch and width are summarized in Table 3.3.

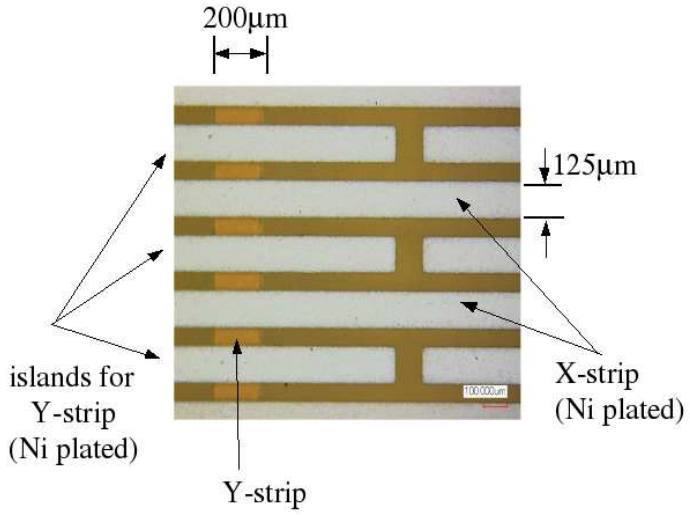

Figure 3.6: A photograph of the readout board (BVH type)

Table 3.2: The pitch, the width and the length of the X and Y strips (BVH-type)

strip	pitch (μm)	width (μm)	length (μm)
X	350	125	-
Y	1400	200	-
islands for Y	350	125	1300

Table 3.3: The pitch, the width and the length of the X and Y strips (single side type)

strip	pitch (μm)	width (μm)	length (μm)
X	350	70	-
Y	1400	290	-

3.1.3 Readout electronics

To achieve a position resolution of 100 μm in the X direction and 700 μm for the Y direction, flash ADC readout is necessary for tracks with a finite incident angle. Information of a waveform used in detail analysis is needed in order to calculate a hit position for the tracks with the incident angle. Signals from strips of a GEM tracker were amplified and sampled every 25 ns for 30 clock counts by a preamplifier

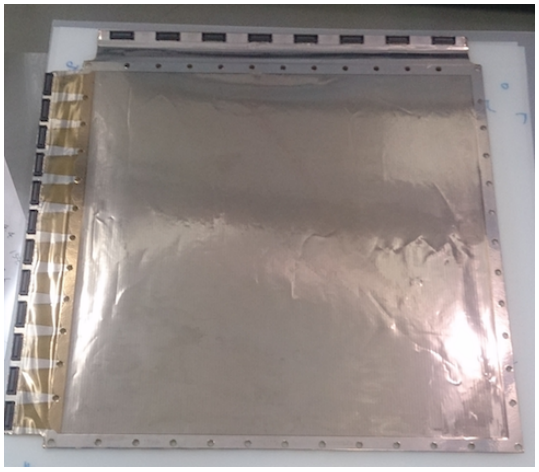

Figure 3.7: A photograph of a 200 × 200 mm^2 readout board (BVH type)

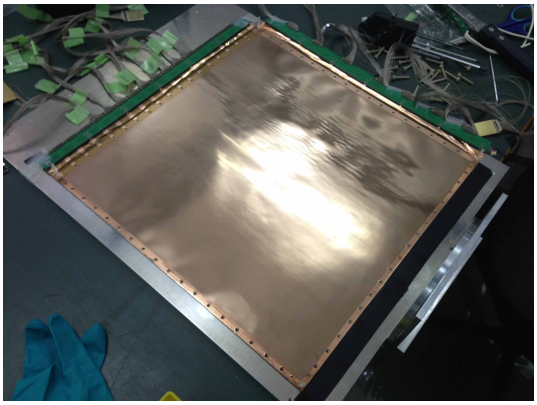

Figure 3.8: A photograph of a 300 × 300 mm^2 readout board (single side type)

hybrid card using the APV25-s1 ASIC [22]. An APV25 chip has 128 channels of low-noise preamplifiers followed by a shaper stage and each channel has an analog memory whose depth is 4 μs with a sampling rate of 40 MHz. A photograph of the card is shown in Fig. 3.9.

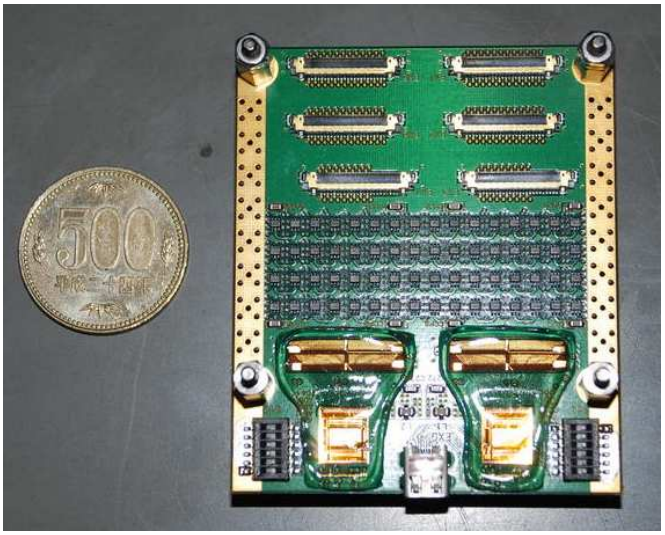

Figure 3.9: A photograph of a preamplifier card using the APV25-s1 chip

3.1.4 High voltage distribution

High voltage is applied to the mesh and three GEM foils by a resistor chain (1 MΩ and 2 MΩ) with protection resistors (10 MΩ) as shown in Fig. 3.10 and Fig. 3.11. In order to be able to change the electric field of drift gap, high voltage supply

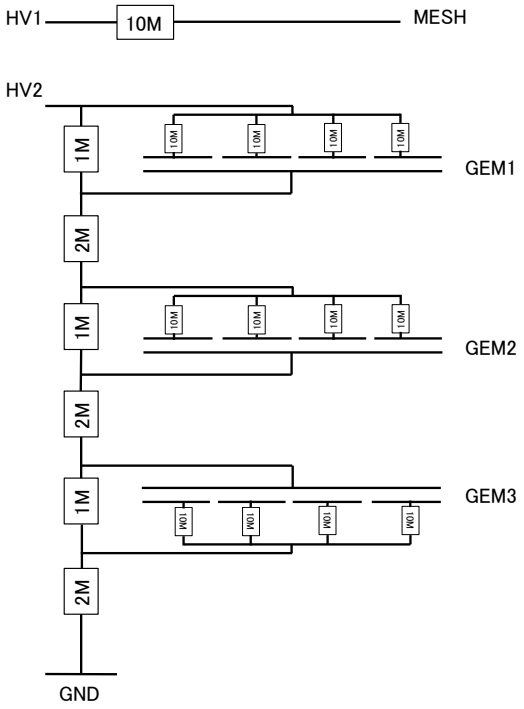

Figure 3.10: 200 GEM HV supply.

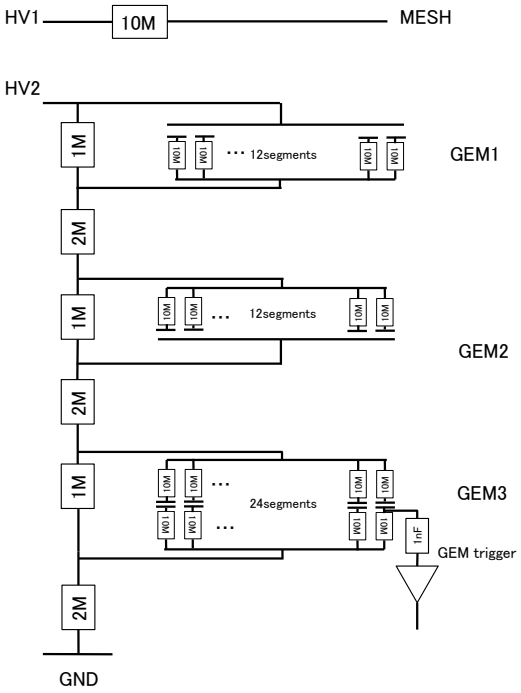

Figure 3.11: 300 GEM HV supply.

is separated between the mesh and the GEM foils. In each $300 \times 300\,\mathrm{mm}^2$ GEM divided into 24, there is a coupling condenser of 1 nF to pick up a signal from foil for trigger.

3.1.5 Trigger

An e^+e^- event trigger consists of three-fold coincidence of GEM trackers, HBDs and LGs. In the GEM tracker, trigger signals are obtained from the cathode plane of the induction gap of $300 \times 300\,\mathrm{mm}^2$ GEM tracker, namely the back side of the last GEM foil in the stack. Assuming the GEM foil structure as a thin gap parallel plate condenser, detector capacitance C_d is expected to be quite large of approximately 50 nF. Considering the detector capacitance and the high rate counting, the size of trigger tiles should be small. Therefore, the GEM foil is divided into 24 segments. Each segment has detector capacitance of 2 nF and its counting rate is expected to be $1 \sim 2$ MHz in the forward region of the spectrometer.

A new Amplifier-Shaper-Discriminator (ASD) ASIC with low noise and fast shaping time is developed in order to cope with such a high rate and large input capacitance. Details are described the following chapter.

3.1.6 Material budget

Materials with small atomic number and very thinness need to be used to decrease effect of multiple scattering which makes momentum resolution of trackers worse. Components of the GEM trackers and their radiation length are summarized in Table 3.4 and 3.5.

Table 3.4: The radiation length of a GEM tracker ($100 \times 100, 200 \times 200\,\mathrm{mm}^2$)

components	material	X_0 (cm)	length (μm)	aperture ratio	radiation length (%)
Mesh	Mylar	28.5	25	-	0.0088
	aluminum	8.90	0.2	-	0.0002
GEM	copper	1.44	24	0.195	0.1346
	kapton	28.6	150	0.049	0.0499
Readout	copper x	1.44	2	0.311	0.0192
	copper y	1.44	4	0.858	0.0040
	kapton	28.6	25	0.01	0.0087
	nickel	1.42	2	0.311	0.0194
Total					0.2448

Table 3.5: The radiation length of a GEM tracker ($300 \times 300\,\mathrm{mm}^2$)

components	material	X_0 (cm)	length (μm)	aperture ratio	radiation length (%)
Mesh	Mylar	28.5	25	-	0.0088
	aluminum	8.90	0.2	-	0.0002
GEM	copper	1.44	24	0.195	0.1346
	kapton	28.6	150	0.049	0.0499
Readout	copper x	1.44	2	0.8	0.0028
	copper y	1.44	2	0.171	0.0116
	kapton	28.6	25	0.8	0.0017
	nickel	1.42	2	0.171	0.0117
	glass epoxy	19.4	100	-	0.05
Total					0.2728

3.2 Signal of GEM tracker

Electrons generated by ionization in the drift gap transport to readout electrodes through GEM and transfer gaps. Each GEM foil multiplies electrons as a factor of 20. At the last gap (induction gap), multiplied electrons generate a signal to readout electrodes. Also, drift of electrons in the gap generates a signal at the last GEM foil.

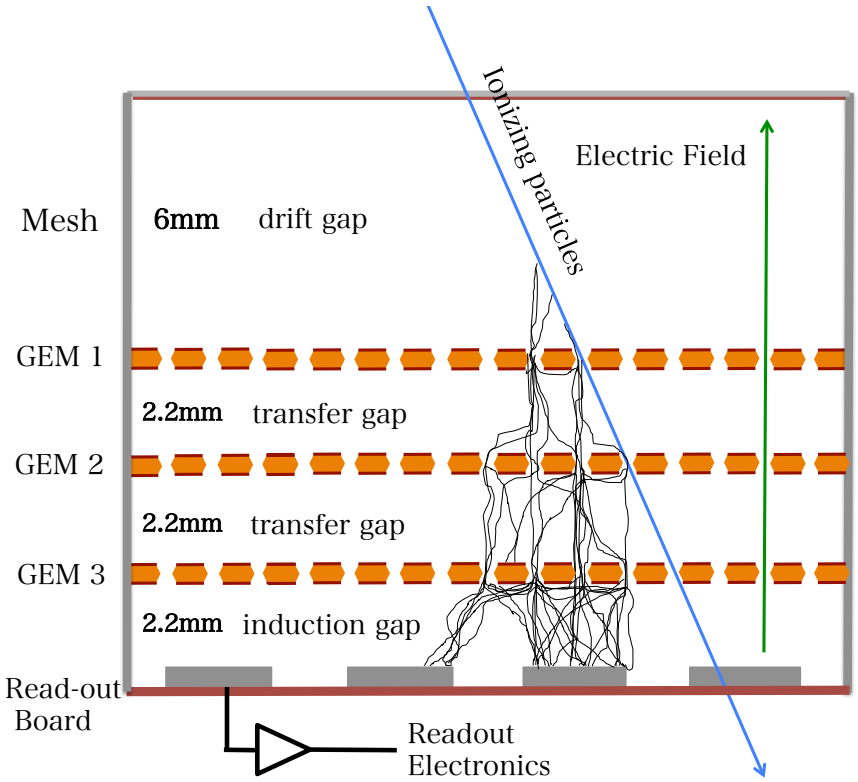

Figure 3.12: The signal process of a GEM tracker.

Chapter 4

Development of GEM trigger

A GEM tracker whose size is $100 \times 100\,\mathrm{mm}^2$ works well with a position resolution of $100\,\mu$m for incident angle of 0° to 30° and high detection efficiency ($\sim 97\%$). Therefore, the next step is development of large GEM trackers, such as $200 \times 200\,\mathrm{mm}^2$ and $300 \times 300\,\mathrm{mm}^2$. Especially, the $300 \times 300\,\mathrm{mm}^2$ GEM tracker generates a trigger signal from the back side of last GEM foil (foil signal).

In this chapter, development of a trigger signal using GEM tracker and related performance test of the large GEM tracker are reported.

4.1 GEM trigger

Considering to pick up a trigger signal from Y strips of the $300 \times 300\,\mathrm{mm}^2$ GEM tracker, a complex electronics which can deal with a signal process for both tracking and trigger is needed. In addition, the $300 \times 300\,\mathrm{mm}^2$ GEM tracker has Y strip channels of 216. Thus, many channels, such as $216 \times 26 = 5616$ in total, is required for the trigger of GEM tracker. However, assuming the foil signal can be used for the trigger of GEM tracker, signal processing of tracking and that of trigger can be separated and, the number of channels for trigger can be decreased. Taking account of the size of the trigger tile which the electron ID detectors of HBD and LG cover, using the foil signal from divided electrodes of GEM foil is suitable for the signal processing of the trigger. Study of the foil signal and its electronics are described in this chapter.

4.1.1 Prototype of the GEM foil trigger

To study basic properties of a GEM foil signal, a $100 \times 100\,\mathrm{mm}^2$ GEM tracker was used since a small tracker works well and is operated easily.

Foil signal of X-ray

The setup of a foil signal test using a X-ray is shown in Fig. 4.1. Effective gain of the size of $100 \times 100\,\mathrm{mm}^2$ GEM tracker is measured by using a 5.9 keV of X-ray from ^{55}Fe. Charge of the foil signal is amplified by a charge sensitive preamplifier whose calibrated gain is about $0.73\,\mathrm{V/pC}$ and time constant τ is $1\,\mu$s as shown in Fig. 4.2.

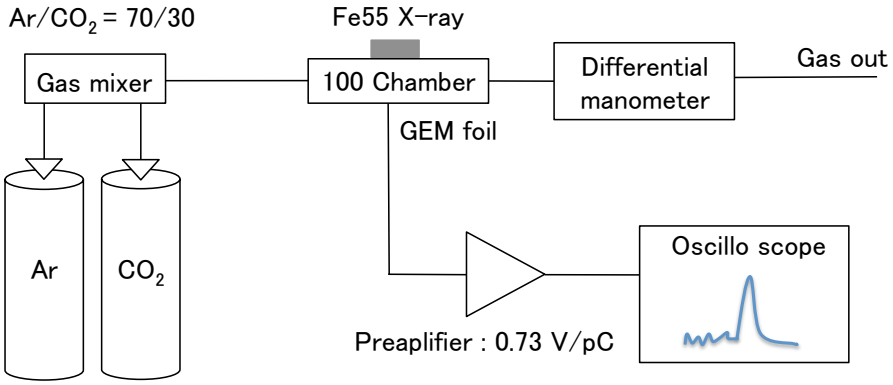

Figure 4.1: Setup of gain measurement by using foil signal

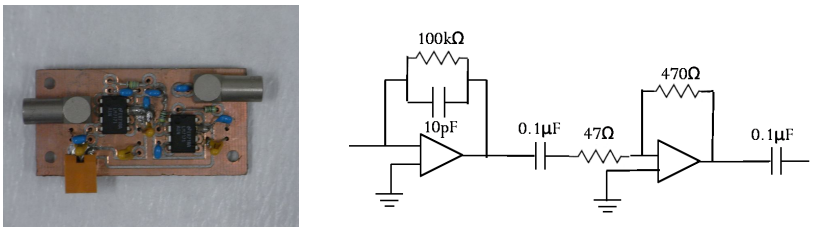

Figure 4.2: A photograph and a schematic of the preamplifier

The data of the signal is taken by using a peak ADC module. The self-trigger mode is used for the data acquisition. A typical shape of the foil signal is shown in Fig. 4.3.

The working function of Ar(70%) and CO_2(30%) is 28.1 eV. Therefore, the number of electrons generated by 5.9 keV X-ray is

$$N_{seed} = 5.9 \times 10^3/28.1 \simeq 210 \tag{4.1}$$

The effective gain G is given by

$$G = \frac{h\,(\mathrm{V})}{0.73\,(\mathrm{V/pC}) \times N_{seed} \times 1.6 \times 10^{-7}(\mathrm{pC})} \tag{4.2}$$

where h (V) is pulse height of the amplified signal. An example of energy spectrum detected by the GEM tracker is shown in Fig. 4.4. The full energy deposit peak and the escape peak can be seen clearly. The gain can be calculated from the ADC value of the main peak. The result of gain measurement is shown in Fig. 4.5. Not only the anode side of GEM tracker, such as strip or pad readout, also the cathode side can be used for gain measurement.

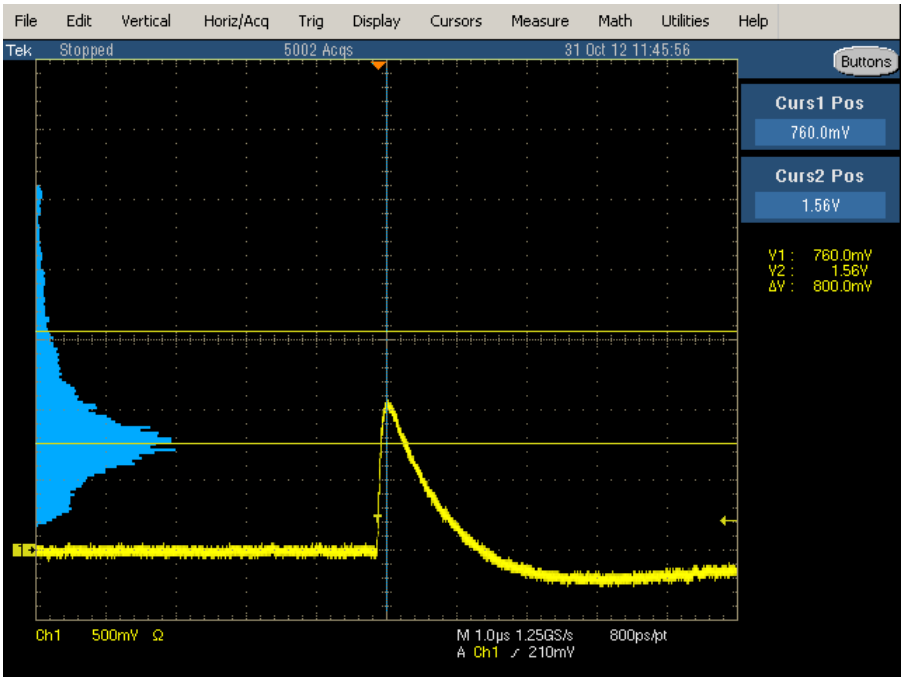

Figure 4.3: A waveform of the foil signal

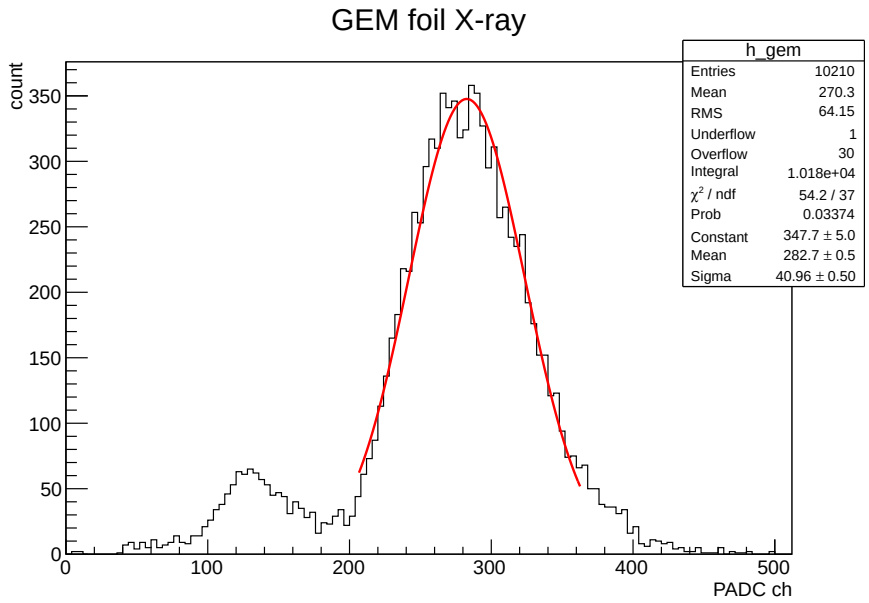

Figure 4.4: Energy spectrum of ^{55}Fe

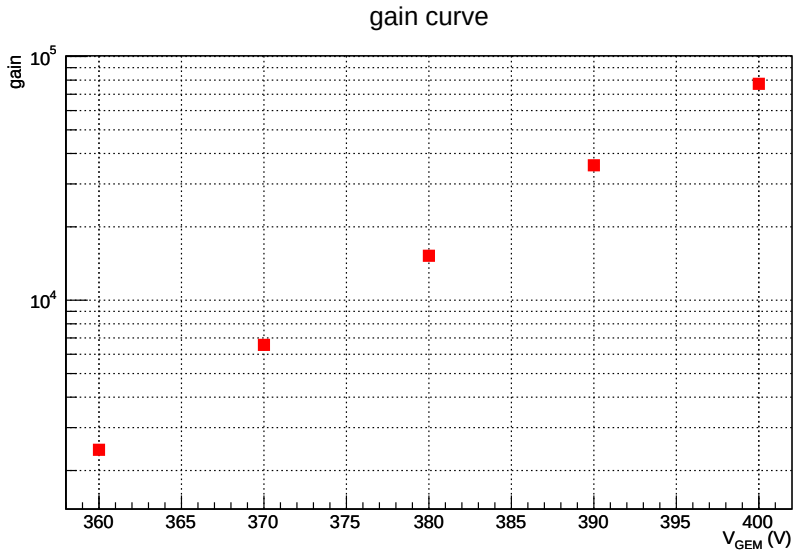

Figure 4.5: Gain vs applied high voltage across each GEM

Foil signal of charged particle

A test experiment was performed at the J-PARC K1.1BR beam line in December 2012 and January 2013. In the test experiment, efficiency of the prototype GEM foil trigger was evaluated by using e^- or π^- beam with a momentum of 1.0 GeV/c. The GEM tracker was placed between two trigger scintillators ($3 \times 3\text{cm}^2$). The setup is shown in Fig. 4.6. A peak ADC module was used for the measurement as well as in the case of X-ray.

The trigger efficiency is estimated through the following steps.

1. Evaluate pedestal value and its sigma for the foil signal in a pedestal run (clock trigger run) to estimate noise level as shown in Fig. 4.7 .

2. Measure a spectrum obtained by a beam run and evaluate the charge sum after amplification by GEM.

3. Define the efficient event as a event in which the ADC value is larger than threshold value (pedestal mean $+ 3 \times \sigma$) and count it as shown in Fig. 4.8.

In this analysis, e^- and π^- are regarded as separated samples which are differ in energy deposit. The electron identification can be performed by using the ADC value of gas Čerenkov counters (GC1 and GC2) placed at forward of the GEM tracker.

In Fig. 4.8, the spectrum of hadronic particles is well fitted with a Landau distribution. The charge amplified by triple-GEM is estimated by calculating the mean of the distribution of the ADC value. The charge Q is given by

$$Q\,(\text{pC}) = \frac{h\,(\text{mV}) \times 10^{-3}}{0.73\,(\text{V/pC})} \tag{4.3}$$

where h is pulse height of the foil signal which can be calculated from the ADC value corresponding to the mean of the distribution and 0.73 (V/pC) is a calibrated gain of the preamplifier used in this measurement. The number of total events for each run N_{tot} is defined as a count of coincidence signal of S1 and S2. The number of efficient events N_{eff} is given by calculating an integral of events which satisfy

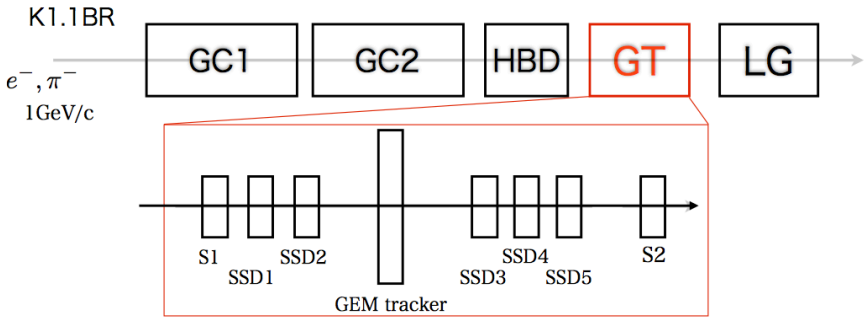

Figure 4.6: Setup of the test experiment

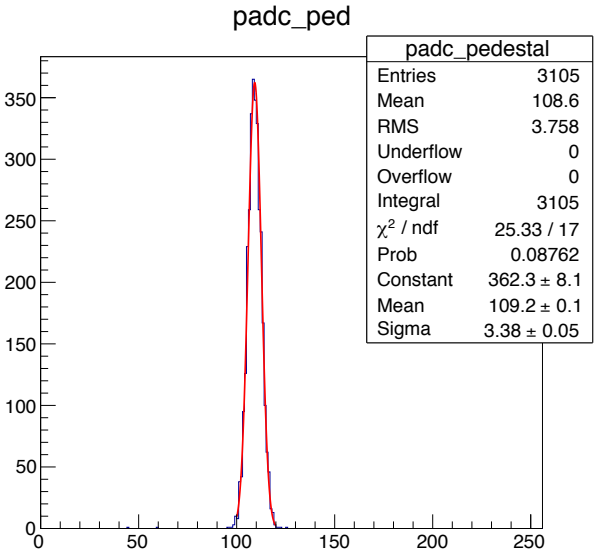

Figure 4.7: Evaluation of pedestal and its sigma.

with the ADC value $>$ (pedestal mean $+ 3\sigma$). Therefore, the trigger efficiency ϵ is evaluated by

$$\epsilon = \frac{N_{\text{eff}}}{N_{\text{tot}}} \tag{4.4}$$

In the case of Fig. 4.8, the efficiency for hadrons is about 97% and that of electron is over 99%.

Changing conditions, such as operation voltage of GEM, an incident angle of particle and a drift gap of the GEM tracker, which corresponds to changing the number of ionized electrons and gain, the charge given by (4.3) and the trigger efficiency are evaluated at run by run. Dependence of the efficiency on the charge is plotted as shown in Fig. 4.9. The relation between the charge and the efficiency is determined almost uniquely. The trigger efficiency of better than 99% is achieved with the charge of larger than 0.15 pC at the mean value of the distribution in this configuration. When the drift gap is 6 mm, the number of ionized electrons n_{seed} by the beam is estimated as following,

$$n_{seed} = (\frac{dE_{\text{Ar}}}{dx} \times 0.7 + \frac{dE_{\text{CO}_2}}{dx} \times 0.3) \times 0.6/W \simeq 60 \tag{4.5}$$

where $\frac{dE_{\text{Ar}}}{dx}$ and $\frac{dE_{\text{CO}_2}}{dx}$ are an energy loss in Ar gas and CO_2 gas, W is the working function of the gas mixture. Therefore, the effective gain needed for the efficiency of over 99% is $0.15/(60 \times 1.6 \times 10^{-7}) \sim 1.5 \times 10^4$ in this configuration.

In the E16 experiment, the counting rate becomes $1 \sim 2$ MHz at the forward region where the $300 \times 300\,\text{mm}^2$ GEM tracker is placed. The preamplifier used in the measurement has a long pulse width such as $2\,\mu s$, and hence it can not cope with the high rate counting. A preamplifier with a short pulse width under ~ 500 ns needs to generate trigger signals properly. However, a signal-to-noise ratio decreases as the pulse width or the time constant becomes short. In an aspect of the ratio,

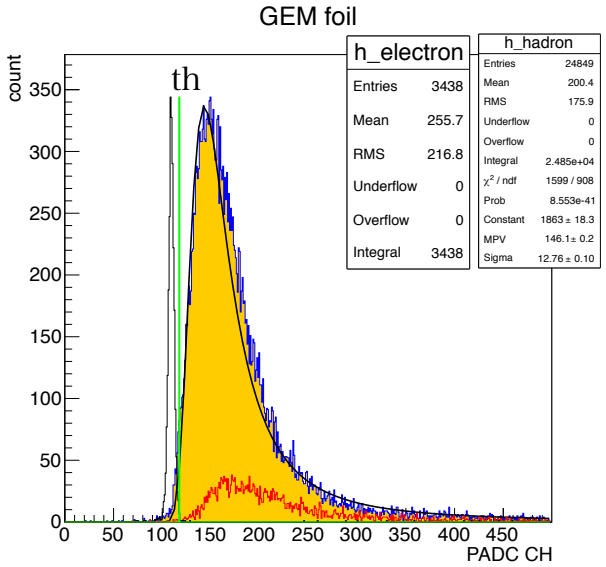

Figure 4.8: The spectrum obtained by a beam run. The black line is pedestal, the green line is threshold value, the blue line is the spectrum of hadronic particles and the red line is the spectrum of electron.

an Application Specific Integrated Circuit (ASIC) is expected to be suitable for electronics of the foil trigger since it has a low-noise property.

To confirm effectiveness of using an ASIC as a low-noise preamplifier, the trigger efficiency is evaluated by using an ASIC designed for the strip signal the same as by the discrete preamplifier. Figure 4.10 shows comparison between the ASIC and the discrete preamplifier at the same operation voltage of GEM. Though the ASIC is not optimized for the foil signal, the signal-to-noise ratio of the ASIC is better than that of the preamplifier. In case of the gain of $\sim 10^4$, the trigger efficiency reaches $\sim 99\%$ by using the ASIC.

In conclusion, the GEM foil signal can be used as the trigger of the GEM tracker. Using a ASIC which is optimized for the foil trigger is expected to have good performance.

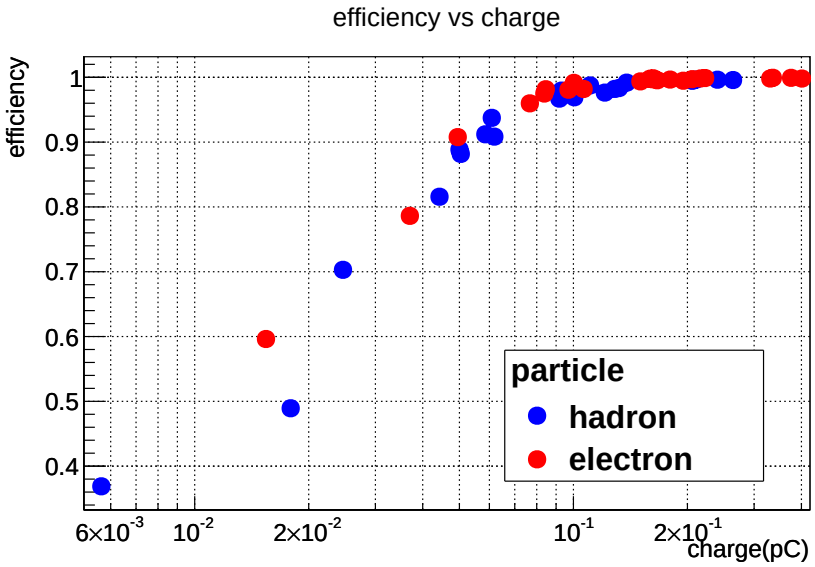

Figure 4.9: The charge dependence of the trigger efficiency.

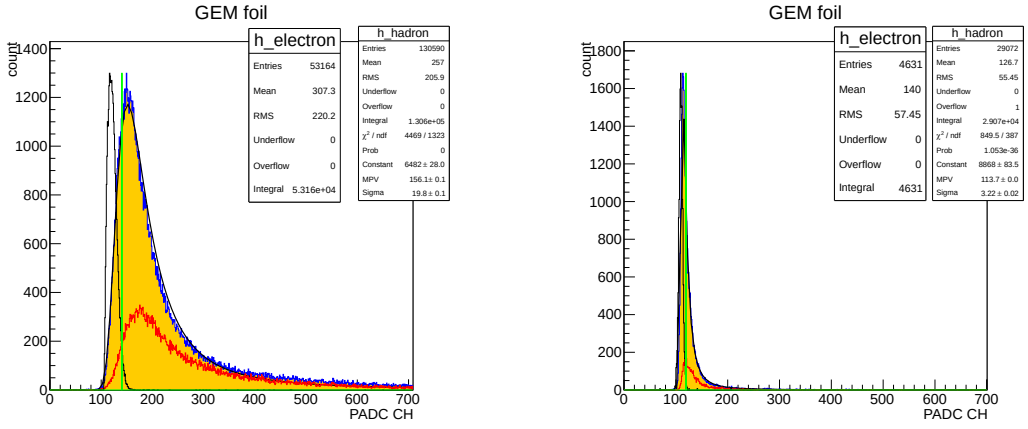

Figure 4.10: The comparison between the ASIC (left) and the discrete preamplifier (right) at the same operation voltage ($V_{\mathrm{GEM}} = 360\,\mathrm{V}$)

4.1.2 Development of the new ASIC

GOTA (GEM Foil Trigger Tracker) is a 6-channel mixed analog-digital ASIC developed to readout the GEM foil signal of the GEM tracker. It is designed in the MXIC 0.5 μm process technology. Each analog channel is made of a charge amplifier, a shaper and a discriminator. The digital section contains a 8-bit register for control of a comparator on-off, a polarity of the comparator and an adjustment of each threshold.

To develop the ASIC for the GEM foil trigger, we determined a specification of the ASIC and simulated its electric circuit to confirm it satisfy the specification. The specification is summarized in Table 4.1. Then the performance of the prototype ASIC is tested and compared with the result of the simulation.

Determining the dynamic range of the ASIC

Assuming that the effective gain of the GEM tracker is 10^4, a suitable dynamic range of the ASIC is evaluated. The minimum charge keeping the trigger efficiency larger than 99% is estimated by calculating the number of ionized electrons in the drift gap by using Garfield++. Here, the efficiency ϵ is defined as

$$\epsilon = \frac{1}{N_{\text{entry}}} \sum_{n=n_{\text{min}}} L(n) \tag{4.6}$$

where N_{entry} is the number of total events, n_{min} is a threshold which can be detected by the ASIC and $L(n)$ is a distribution of the number of ionized electrons.

The situation which makes the mean of the number of ionized electrons minimum is the condition that the drift gap is 3 mm, the incident angle is 0° and the momentum of the electron is 0.4 GeV/c. The reason of assuming 3 mm gap is that there remains possibility using 3 mm gap because of high rate capability. In this condition, the distribution $L(n)$ is shown as the left side of Fig. 4.11. The right side of Fig. 4.11 is the case of drift gap of 6 mm. The dependence of the efficiency on the threshold can be estimated from the distribution and is plotted in Fig. 4.12 for the 3 mm drift gap and the 6 mm. In order to achieve the trigger efficiency of 99% in the 3 mm gap case, the ASIC must be able to pick up a charge of $6 \times e \times 10^4 \simeq 10$ fC to distinguish a signal from noise. A factor of 3 is required between a minimum signal and noise. The noise should be $2 \times 10^4 e$ (ENC).

Table 4.1: Chip characteristic

N channels	6
chip size	$5.2 \times 2.6\,\text{mm}^2$
preamplifier gain	$3.6\,\text{mV/pC}$ ($C_{\text{det}} = 2\,\text{nF}$)
shaper time constant	25 ns
ENC	$2 \times 10^4 e$
power supply	$\pm 2.5\,\text{V}$

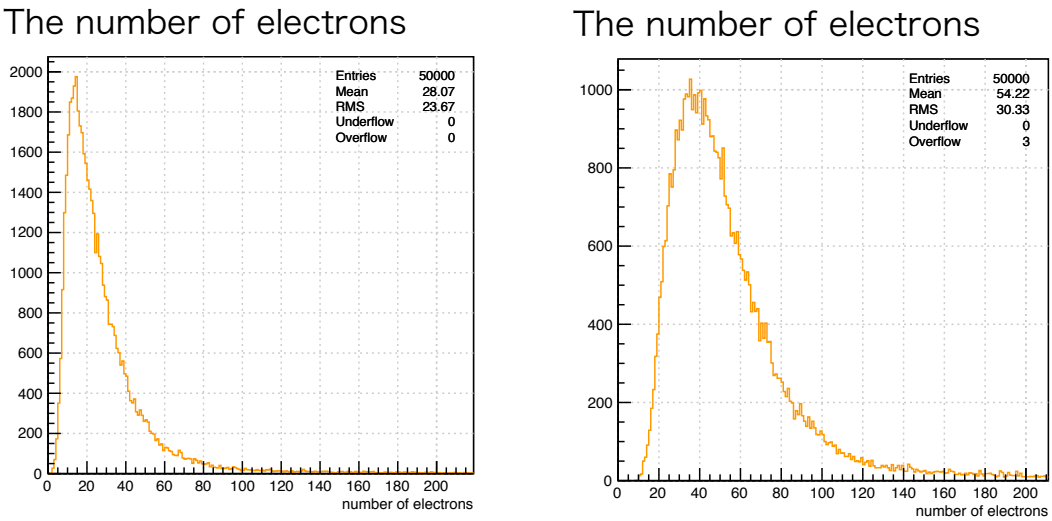

Figure 4.11: The distribution of the number of ionized electrons (left: $d = 3\,\mathrm{mm}, 0°, p_e = 0.4\,\mathrm{GeV}$, right: $d = 6\,\mathrm{mm}, 0°, p_e = 0.4\,\mathrm{GeV}$)

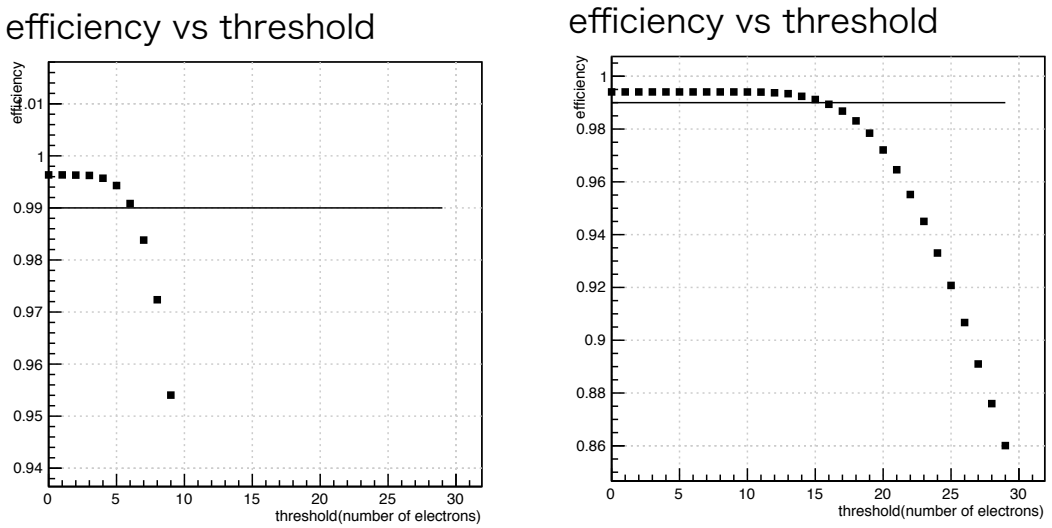

Figure 4.12: The dependence of the efficiency on the threshold (left: $d = 3\,\mathrm{mm}, 0°, p_e = 0.4\,\mathrm{GeV}$, right: $d = 6\,\mathrm{mm}, 0°, p_e = 0.4\,\mathrm{GeV}$)

Simulation of the electric circuit

The basic structure of the electric circuit is provided by Open-It [23]. The electric circuit is checked by a simulation whether it satisfies a required specification and is modified repeatedly.

Architecture of an analog channel is made of four blocks, such as a charge sensitive preamplifier, a pole-zero-cancellation (PZC) stage, a shaper and a comparator (discriminator). The charge sensitive preamplifier plays a role of integrating input charge into a voltage. The PZC stage shortens the decay time constant of the charge sensitive preamplifier. The shaper provides noise filtering, amplifying and shaping a waveform in the critical damping condition Its block diagram is shown in Fig. 4.13. The threshold of the comparator is controlled by the digital section.

A signal-to-noise ratio for the expected minimum charge input is evaluated by simulation. As shown in Fig. 4.14, an output signal of the shaper for a 10 fC input test pulse with 2 nF detector capacitance is simulated. The total pulse width is about 200 ns and the pulse height is 36 mV. At the same time, a noise level is also estimated by the simulation, and a noise spectrum is shown in Fig. 4.15. From the spectrum $N(f)$ where f is a frequency, the noise level is calculated by

$$\text{noise level} = \sqrt{\int_{f_{\min}}^{f_{\max}} [N(f))]^2 \, df} \tag{4.7}$$

where $f_{\min}$ and $f_{\max}$ are a lower and a upper limit of the integral respectively. The shaper output has a noise level of $\sim$ 9 mV in this circuit configuration. Thus, a signal-to-noise ratio becomes 4 for the expected minimum charge input and, this value is sufficient for the GEM trigger.

Linearity of the shaper output is checked by varying a input charge in a range from 10 fC to 2×10^3 fC. Figure 4.16 and Figure 4.17 show a relation between input charge and pulse height of the shaper for a relatively lower region of input charge and for a wide range respectively. This circuit has good linearity for typical input charge in the practical operation of the tracker. Thus, gain of this preamplifier is

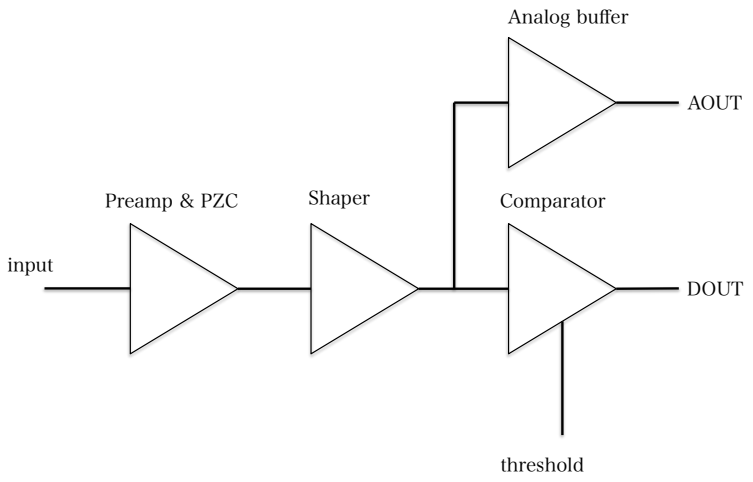

Figure 4.13: A schematic of the GOTA analog section.

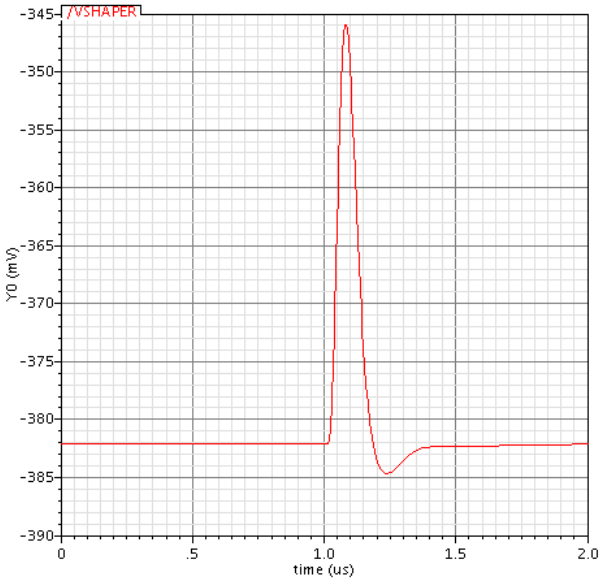

Figure 4.14: A schematic of the GOTA analog section.

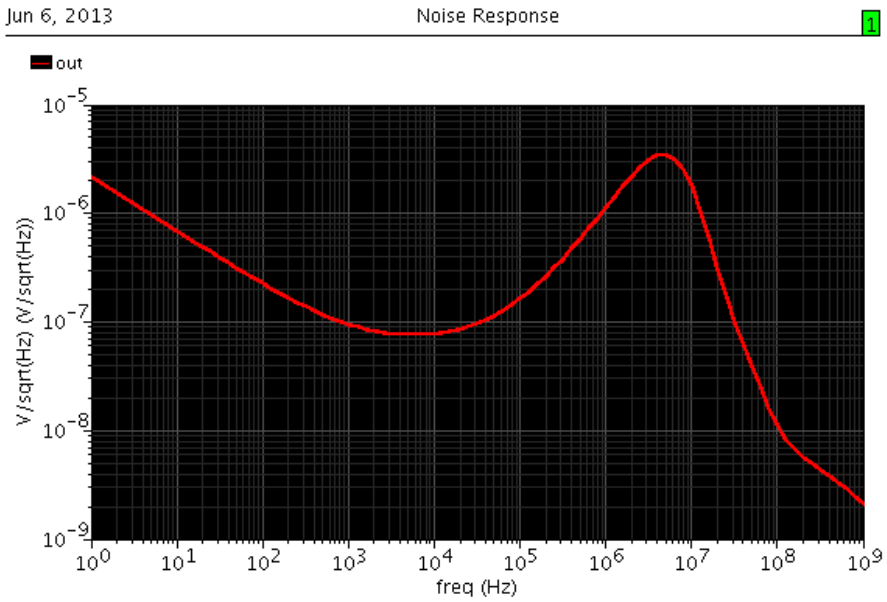

Figure 4.15: A noise spectrum of the shaper output.

estimated to be 3.6 mV/fC from the fitting parameter and, Equivalent Noise Charge (ENC) corresponds to $1.5 \times 10^4\, e$. Without any correction, a threshold level can be selected according to operation status of the tracker, such as applied voltage and a drift gap, due to the linearity. The pulse height starts to be saturated around an input charge of 900 fC because of limitation of power supply. Considering to pick up a trigger, the saturation does not matter since the trigger signal is discriminated by the comparator.

The ASIC is expected to have a narrow pulse shape ($\sim$ 200 ns) and a good signal-to-noise ratio in spite of large detector capacitance of GEM foil, such as $\sim$ 2 nF.

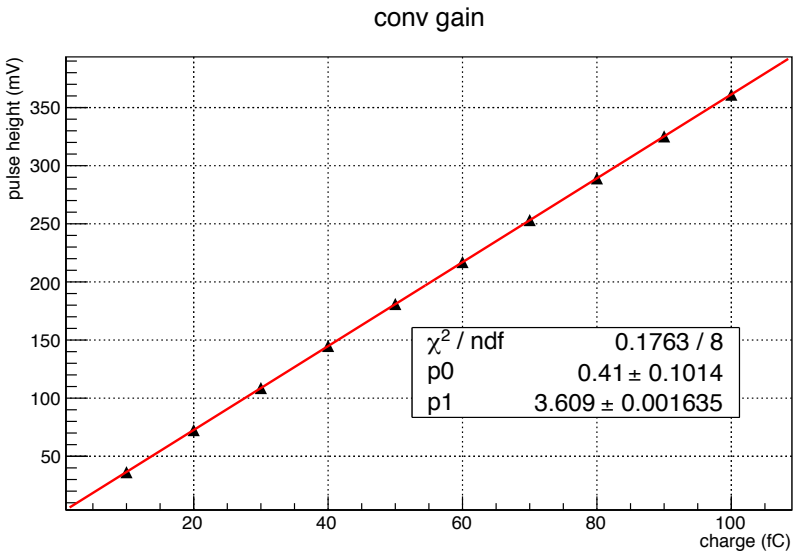

Figure 4.16: A plot of the preamplifier gain (linearity).

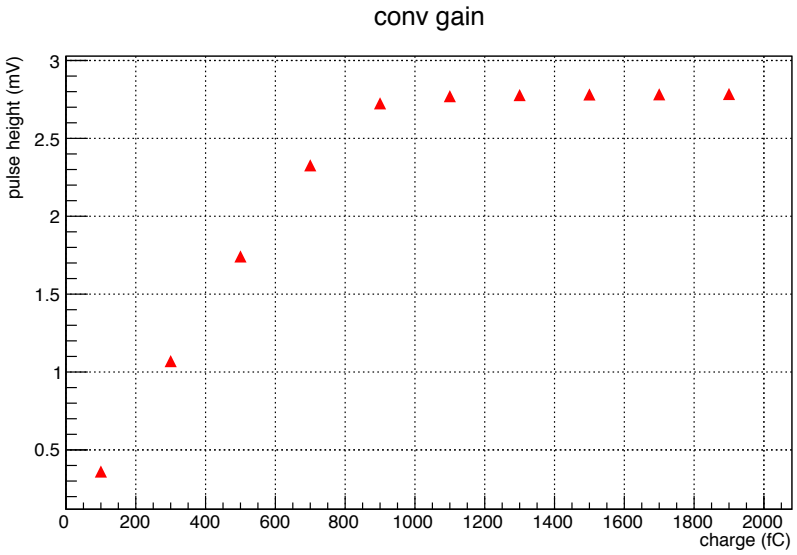

Figure 4.17: A plot of the preamplifier gain (saturation).

The ASIC chip test

Performance of a developed ASIC chip was evaluated. Figure 4.18 and Figure 4.19 show a layout and a photograph of the chip respectively. To evaluate the chip performance, a test board is prepared as shown in Fig. 4.22. This test board has 6 channel input (LEMO), 6 channel analog output (LEMO), 6 channel digital output (pin) and digital control section. A property of an analog signal, such as a pulse shape, a noise level and gain of the ASIC is tested.

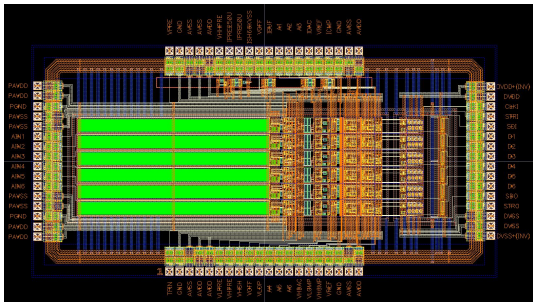

Figure 4.18: A layout of a GOTA chip.

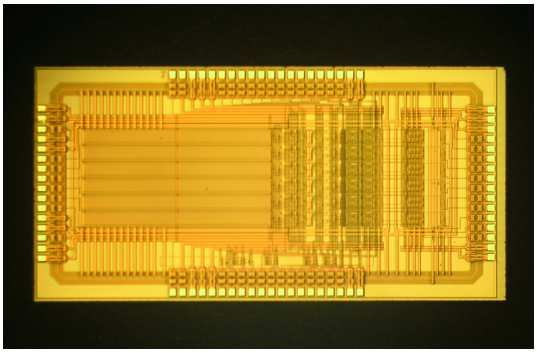

Figure 4.19: A photograph of a GOTA chip.

Figure 4.20 and Figure 4.21 show pulse shapes of the analog output for test pulse input corresponding to charge of 10 fC and 100 fC. The pulse width is about 200 ns as well as the simulation value and the noise level is about 10 mV. Then, gain of the ASIC is measured by a probe as shown in Fig. 4.23. There remains a difference between the simulation and the probe measurement. The difference is caused by deficiency of capability driving signal in an analog buffer inside the ASIC.

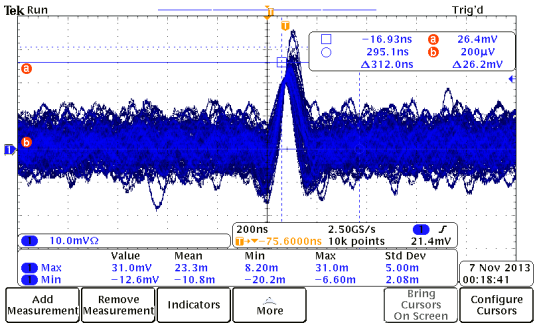

Figure 4.20: Analog buffer output for 10 fC input pulse.

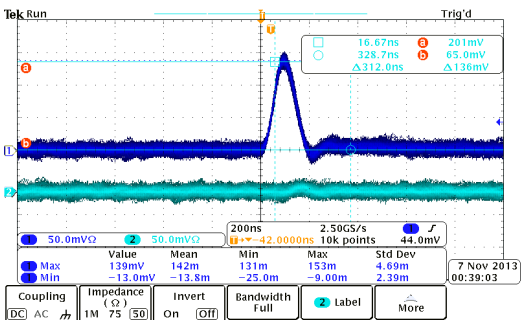

Figure 4.21: Analog buffer output for 100 fC input pulse.

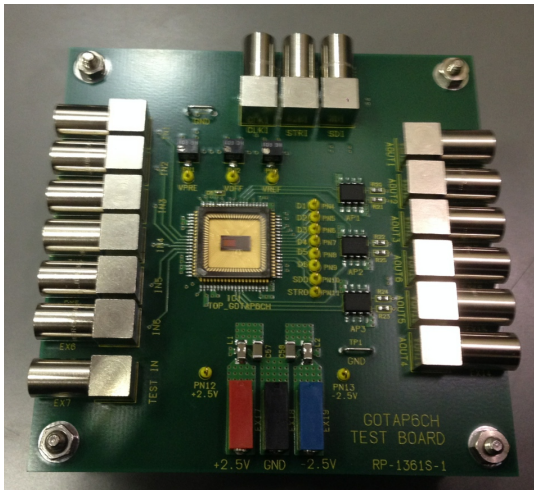

Figure 4.22: A test board of a GOTA chip.

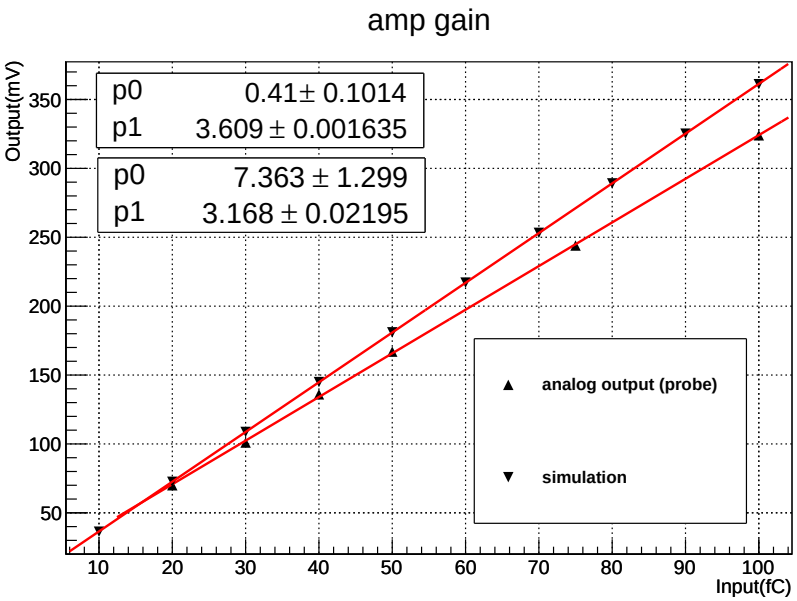

Figure 4.23: Preamplifier gain.

4.2 Laboratory test

A result of laboratory tests for the $300 \times 300\,\mathrm{mm}^2$ GEM tracker is described in this section. The evaluation properties are followings,

- Measurement of effective gain for the GEM tracker as a validation.
- A readout of the foil signal by using a GOTA chip.
- Checking a quality of a $300 \times 300\,\mathrm{mm}^2$ readout board.

4.2.1 Gain measurement for the large GEM tracker

The setup of effective gain measurement is shown in Fig. 4.24. The effective gain is evaluated by using ^{55}Fe as an X-ray radiation source. As shown in Fig. 4.25, a pad readout board is used for this measurement. The pad size is $16 \times 16\,\mathrm{mm}^2$. The GEM tracker stacks a GEM foil divided by 24 as the last GEM in order to test its performance and monitor the foil signal. The gain is measured at nine of the pads to examine position dependence of the gain. Figure 4.27 shows an example of energy spectrum measured at the center of the pads. The main peak and the escape peak can be seen. The gain is calculated from the main peak as the same way of the foil signal in Section 4.1.1, p.23. The result is shown in Fig. 4.28.

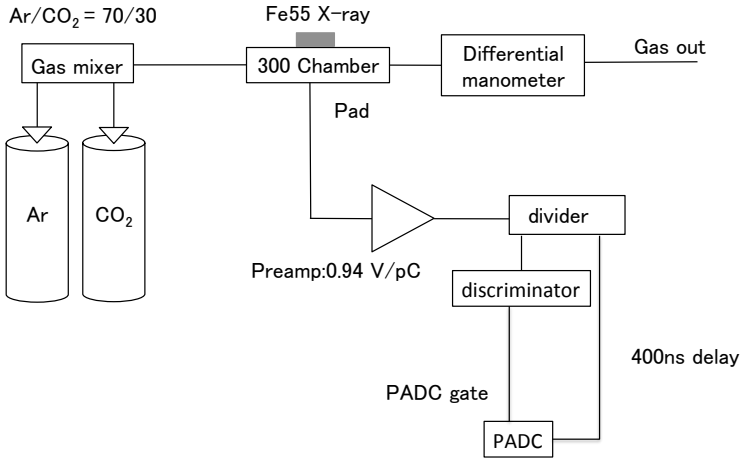

Figure 4.24: A schematic of the setup for gain measurement.

In Fig. 4.28, an identification of pad position (i, j) is defined as shown in Fig. 4.29 and the "100" means the gain of a $100 \times 100\,\mathrm{mm}^2$ GEM tracker used in the last test experiment. There is a difference in the gain on each pad position. It ranges less than a factor of 2 in comparison between the minimum and the maximum gain in this measurement. It is considered due to a fluctuation in a hole size of GEM foils. When the GEM tracker is operated practically, applied voltage on each GEM needs to be 380 V or more to achieve the minimum gain of 10^4. The gain of the $300 \times 300\,\mathrm{mm}^2$ GEM tracker is as well as or larger than that of the $100 \times 100\,\mathrm{mm}^2$. From a viewpoint of the effective gain, the large tracker is expected to have a good performance on a position resolution and detection efficiency.

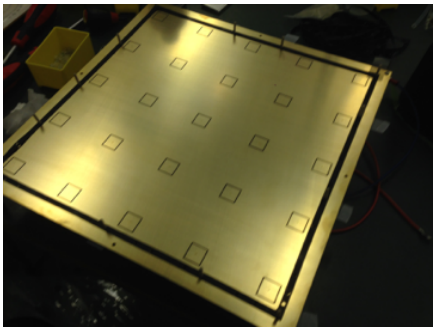

Figure 4.25: A photograph of a pad readout.

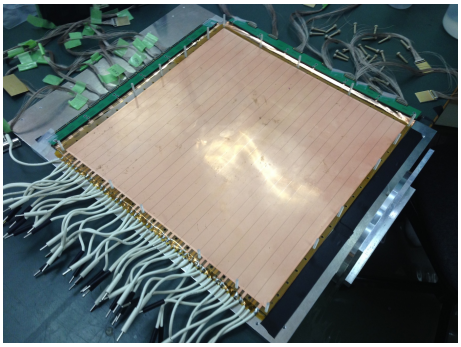

Figure 4.26: A photograph of a $300 \times 300\,\mathrm{mm}^2$ GEM foil divided by 24.

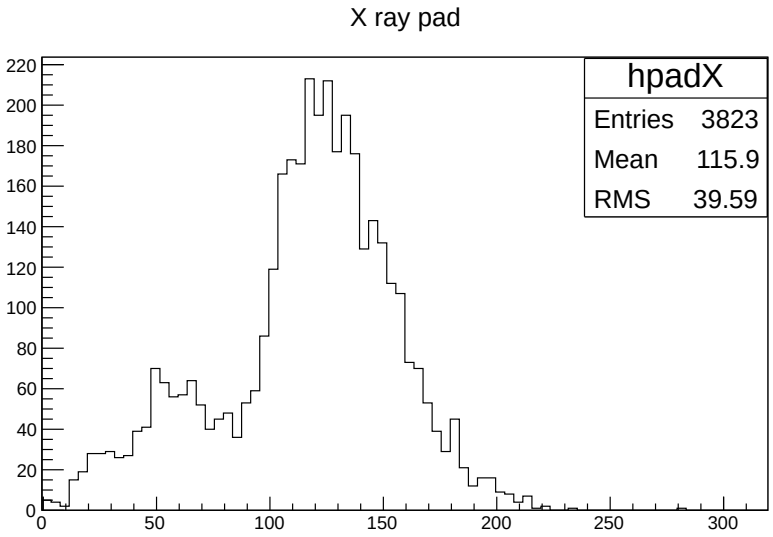

Figure 4.27: Measured energy spectrum of ^{55}Fe

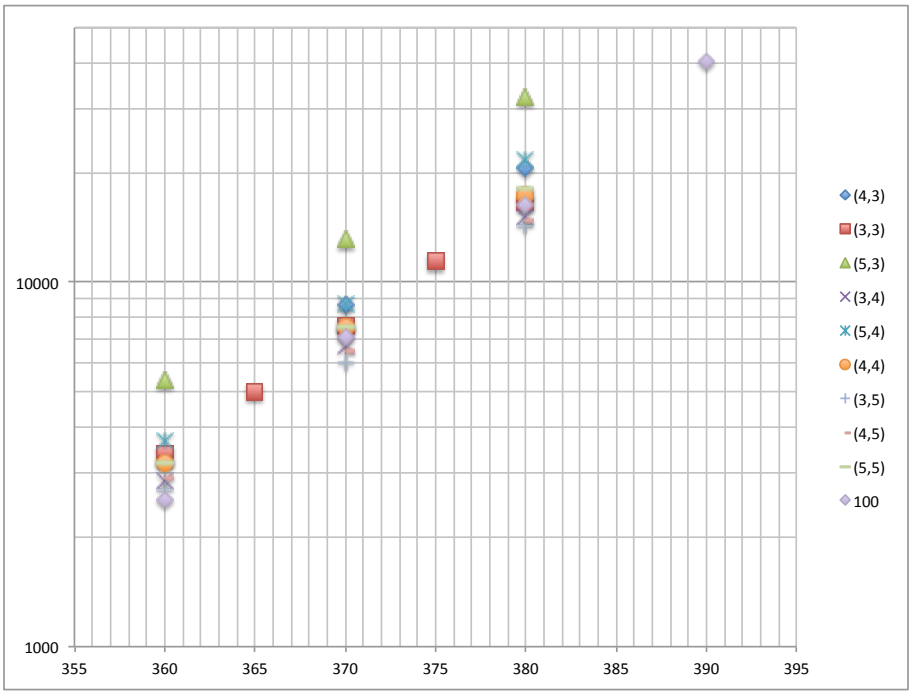

Figure 4.28: The result of gain measurement.

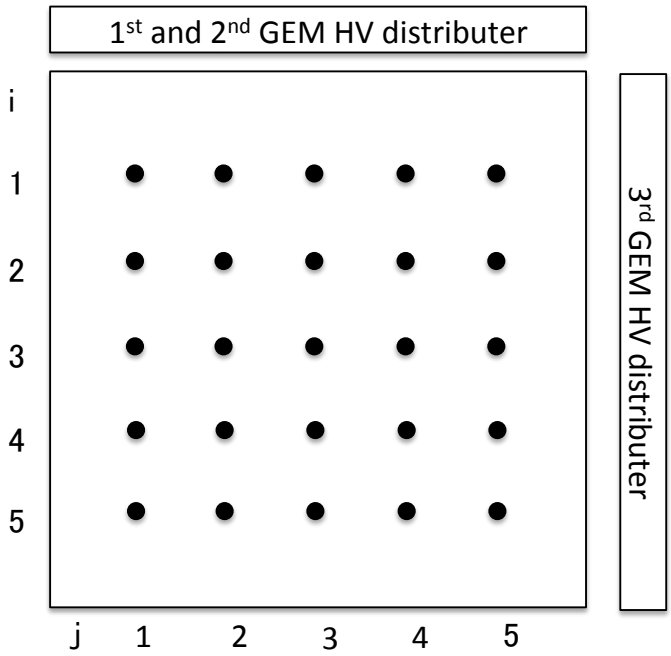

Figure 4.29: The definition of the pad positions.

4.2.2 Foil trigger of the large GEM

Using a GOTA chip, a trigger signal from the last GEM foil was successfully picked up and crosstalk of the trigger signal was evaluated quantitatively by measuring a pulse shape of GOTA chip output using an X-ray. In this measurement, ^{55}Fe is used as the X-ray source. The setup is shown in Fig. 4.30. The foil signal is read out by 4 channels of the GOTA chip, and the pulse shape of each channel is acquired by a flash ADC module (RPV-160) in a condition of self-trigger mode. The main reason why the flash ADC is used in this measurement is to evaluate a quantity of crosstalk in the trigger system. The crosstalk includes effects from both an electric circuit of the ASIC and capacitance among neighboring divided GEM foil electrodes.

An example of waveforms in an X-ray event is shown in Fig. 4.31. One sampling clock of this module equals to 10 ns, and hence the total pulse width is about 300 ns. Each channel of RPV-160 has 8 bits resolution for the full range of $0 \sim -1$ V. The pulse height of FADC 2 in the example corresponds to approximately 250 mV.

The crosstalk is estimated as following steps,

1. Search the maximum for each event of peak and subtract a pedestal. A histogram of the maximum is shown in Fig. 4.32. Also the second largest peak is searched.

2. Calculate a ratio of the second largest value to the maximum value for each event which satisfies the condition that the maximum value is larger than 40 in order to have enough "crosstalked" pulse height at the second peak and avoid chance coincidence made by a noise.

The distribution of the ratio is shown in Fig. 4.33. The crosstalk is estimated to be around 10%, but there is a tail in larger side than 0.1. The tail is originated from a discharge event or charge-sharing one in which two sections of the divided GEM foil have a signal at the same time. Figure 4.34 shows the corrected distribution after using an additional cut which excludes these events.

From above analysis, the crosstalk of the foil trigger system is estimated to be approximately 8% and this level does not give a fatal problem to the system. Still,

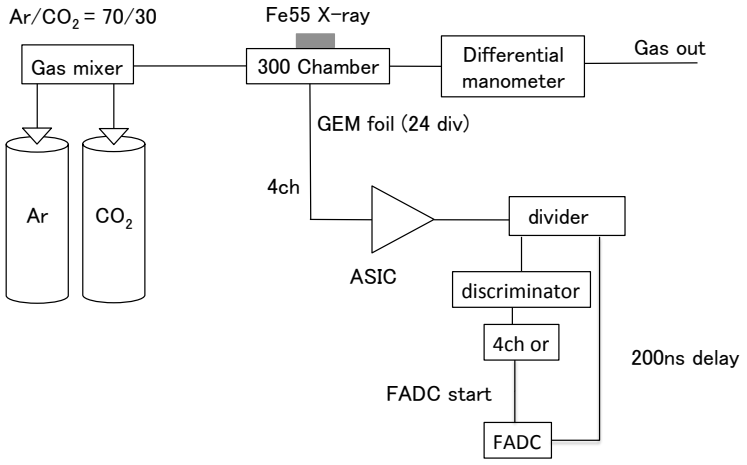

Figure 4.30: A schematic of the setup for gain measurement.

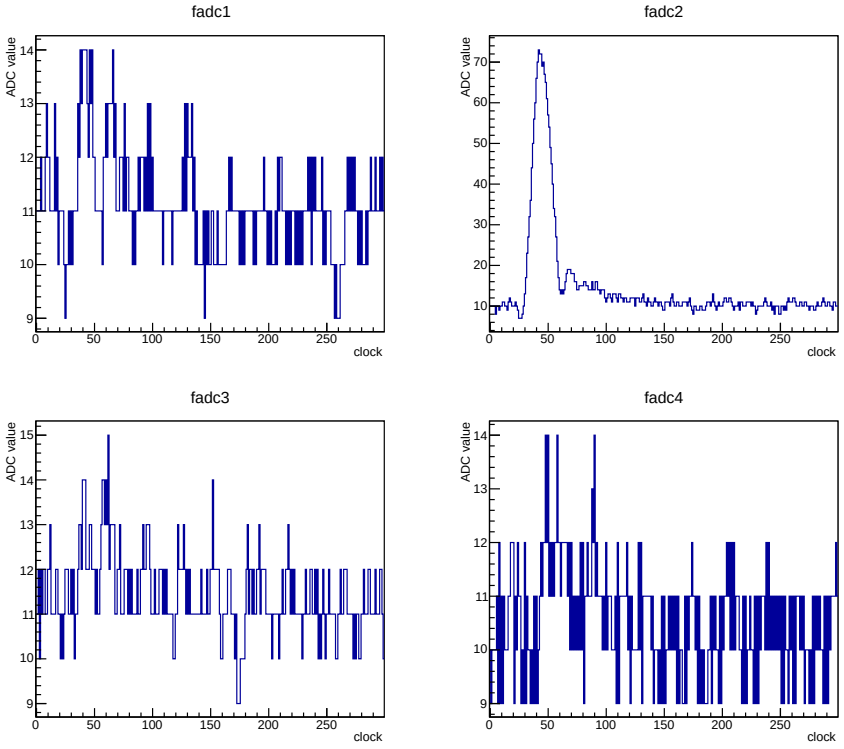

Figure 4.31: Waveforms in a X-ray event. A pedestal of each channel is about 10 channel in ADC value.

the second pulse has 8% of the main pulse and it contains crosstalks of GEM foils and electronics, and effects of noise. The value of 8% is an upper limit for the crosstalk and it is acceptable for the experiment.

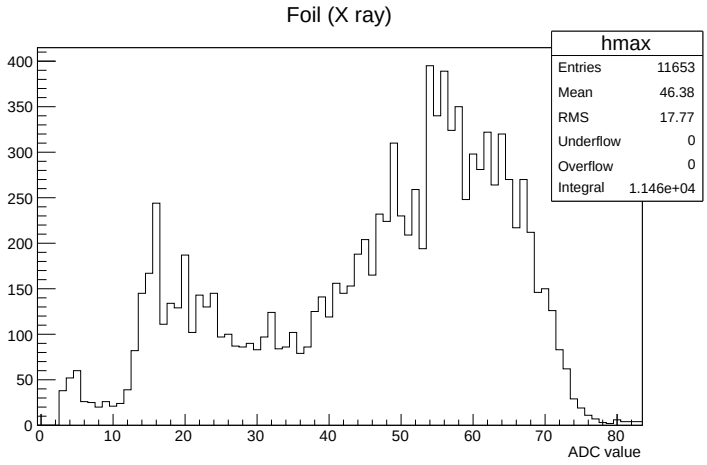

Figure 4.32: The distribution of the maximum ADC value among the 4 channels.

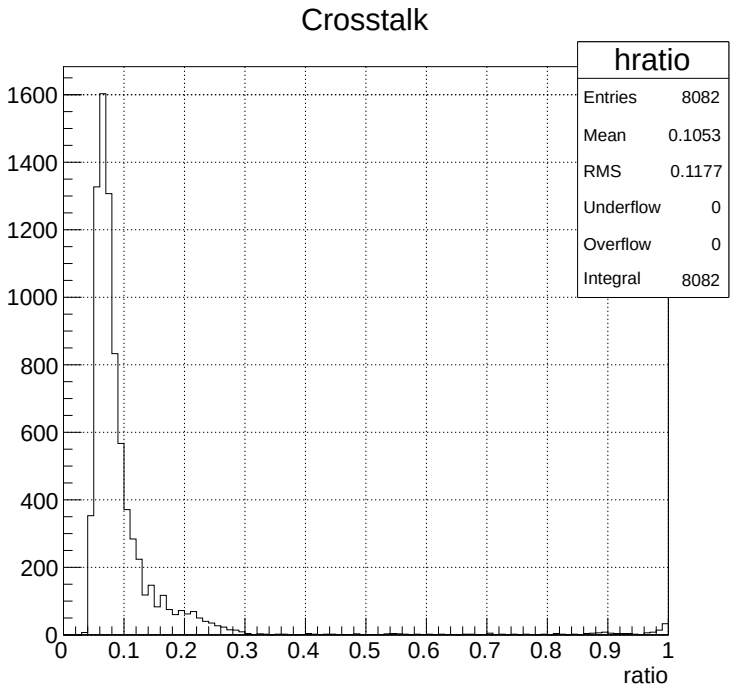

Figure 4.33: The distribution of the ratio.

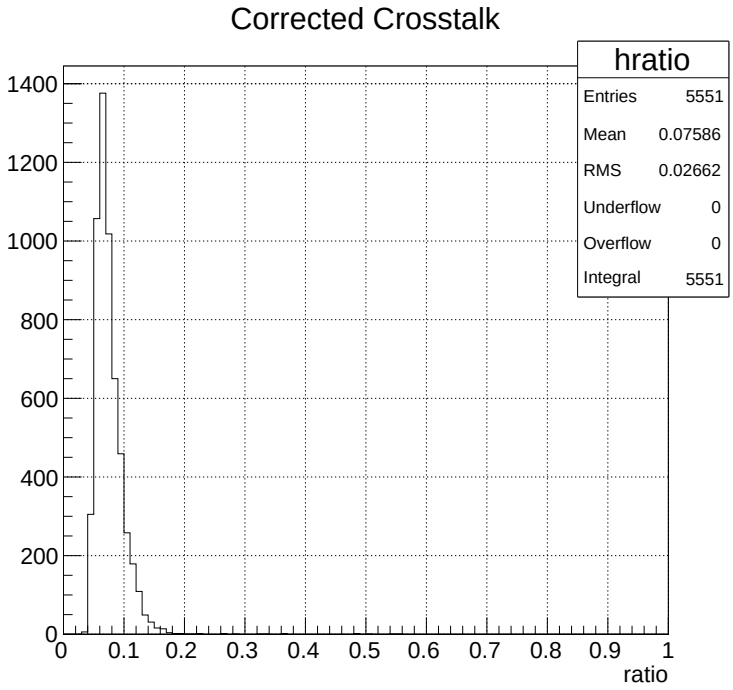

Figure 4.34: The corrected distribution of the ratio.

4.2.3 Test of the large tracker system

A GEM large tracker system was tested by using a APV25 chip and a trigger from a GOTA chip. This setup is a final configuration of the large tracker. It is quite important to operate the large tracker and confirm its performance in this configuration. A response function of X strips was measured as one of properties for the tracker.

The setup is shown in Fig. 4.35. ^{55}Fe is used as a radiation source since localization of ionized electrons generated by the X-ray is suitable for measuring the response function. The measured response function is shown in Fig. 4.36. The distribution is made of a relation with a fraction of charge on a strip and a distance between a hit position and the strip center. Figure 4.37 shows a profile of the response function after cutting events having only one hit strip in order to see a spread structure of charge. The hit position $X_{\rm hit}$ is calculated by

$$X_{\rm hit} = \frac{\sum Q_i X_i}{\sum Q_i} \tag{4.8}$$

where Q_i is charge of the i-th strip and X_i is a position of that. The charge structure for the X-ray in the tracker can be seen, and hence the large GEM tracker is expected to detect a hit position of a radiation by using a trigger from the GOTA chip and strip signals processed by the APV25 chip.

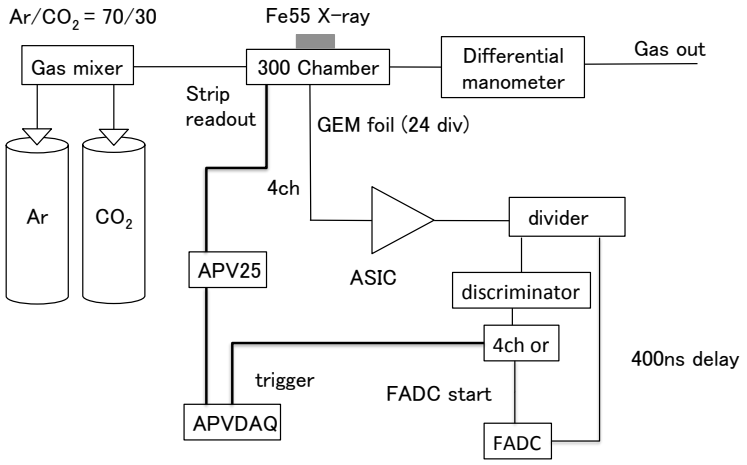

Figure 4.35: A schematic of the setup to measure a response function.

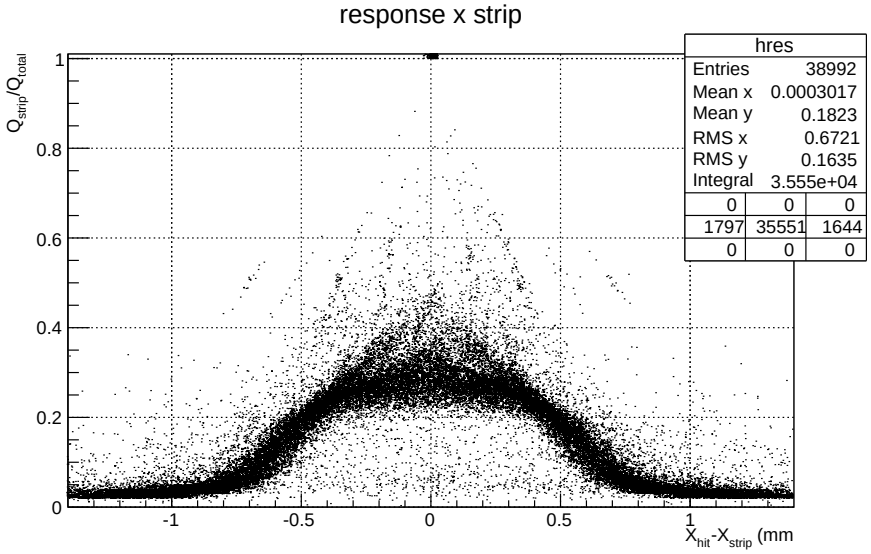

Figure 4.36: A response function of X strips.

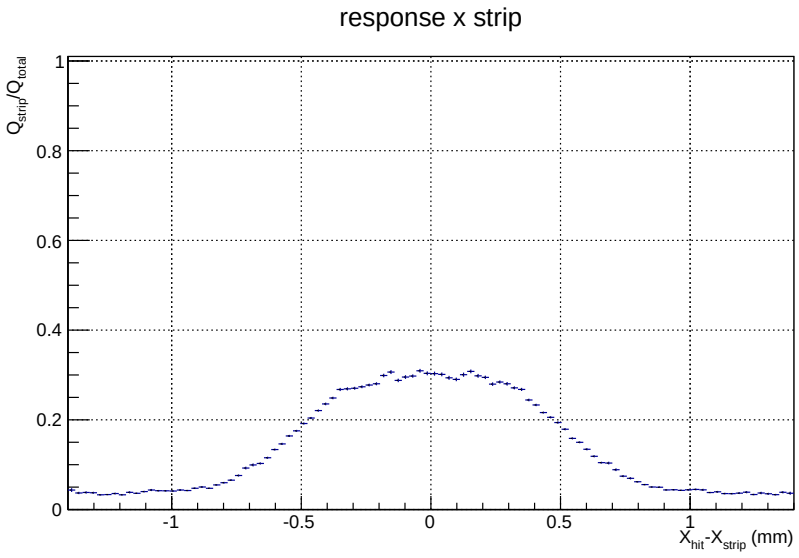

Figure 4.37: A profile of the response function.

Chapter 5

Beam test

A beam test of the large GEM trackers, such as $200 \times 200\,\mathrm{mm}^2$ and $300 \times 300\,\mathrm{mm}^2$, was performed to evaluate a position resolution and detection efficiency. The test was done with a 1 GeV/c positron beam at Laboratory of Nuclear Science (LNS), Tohoku University.

Purposes of the beam test is evaluation of the spatial resolution and the efficiency of the large GEM tracker. The position resolution of a $100 \times 100\,\mathrm{mm}^2$ GEM tracker was achieved under 100μm for an incident angle from 0° to 30° by using an APV25-s1 chip which is a front-end electric circuit of a low-noise ASIC, and optimizing operation gain. In addition, high efficiency was also achieved. Therefore, the next step is to evaluate the performance for the large GEM trackers.

5.1 Test setup

The test setup is shown in Fig. 5.1. Three scintillators, three Silicon Strip Detectors (SSD) and the GEM trackers are aligned along the beam line. The global coordinates is defined as the z-axis equals to the beam axis and, information for positions of detectors along z-axis is summarized in Table 5.1.

A coincidence of three scintillators is used to make a beam trigger. The sizes of the scintillators are $3 \times 3\,\mathrm{cm}^2$, $1 \times 1\,\mathrm{cm}^2$ and $3 \times 3\,\mathrm{cm}^2$ from the upper stream of the beam.

Three SSDs are also installed to determine a reference track. Each SSD gives a hit position in horizontal direction (x coordinate). The strip pitch of them is $80\,\mu$m and there are 384 readout strips. Thus, the sensitive area of SSD is approximately $3 \times 3\,\mathrm{cm}^2$.

5.1.1 Beam line

The test experiment was done with a 1 GeV/c positron beam at the GeV-γ beamline of LNS, Tohoku University. At Linac, pulse beam of electron is accelerated up to 200 MeV and sent to the STB ring. Then the pulse beam is stretched and converted to continuous beam. The beam is boosted up to 1.3 GeV at the STB ring. High energy γ ray ($\sim$GeV) is emitted by bremsstrahlung of accelerated electrons in the STB ring when the electrons cross radiators. The emitted γ ray is converted to an

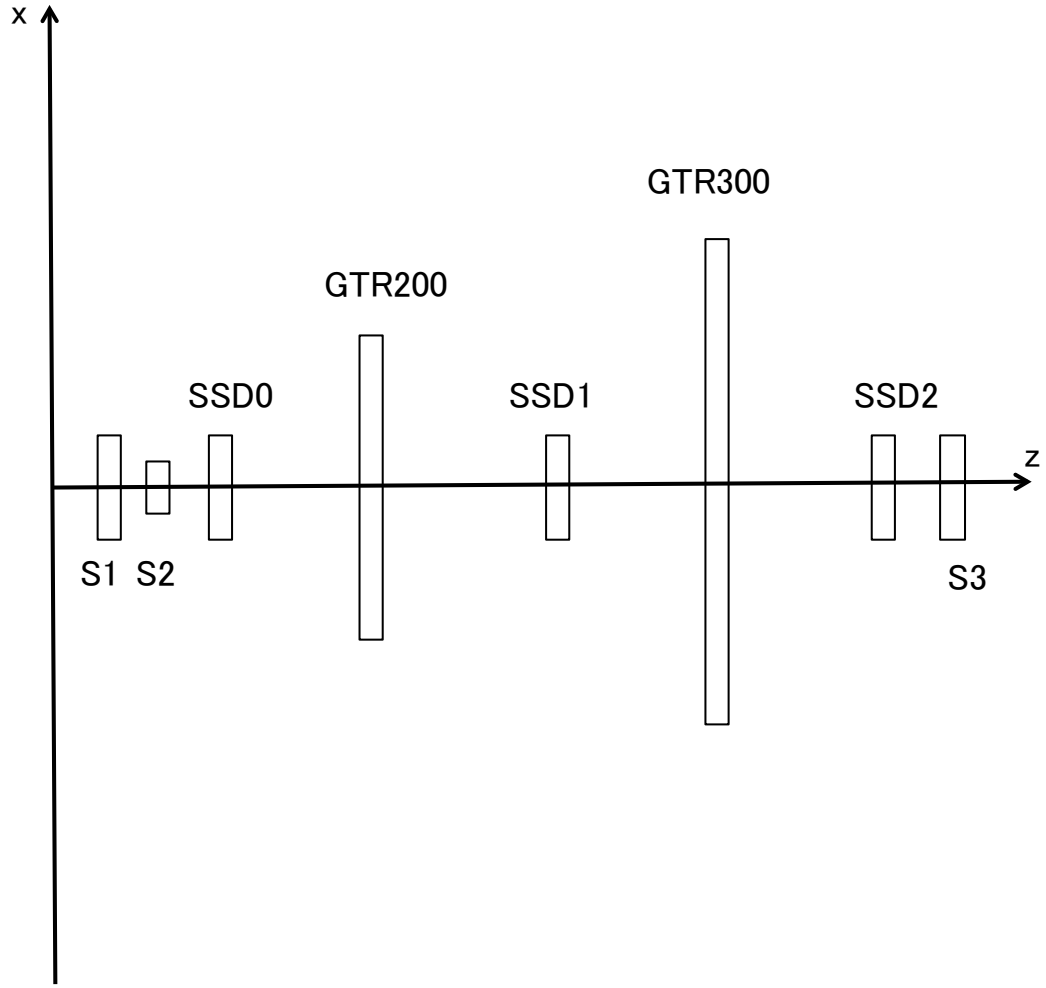

Figure 5.1: The geometry of test setup.

Table 5.1: z component of each detector

detector	z (mm)
SSD0	141.5
SSD1	341.5
SSD2	576.5
GEM tracker 200	218.7
GEM tracker 300	458.7

electron-positron pair at the converter. The generated positron is used as a beam which can be selected by the current of dipole magnet (RTAGX). Momentum of $1\,\mathrm{GeV}/c$ beam is used for the test of the large GEM trackers in the beam test.

5.1.2 DAQ system

For data acquisition, the VME modules were used. The used modules are summarized in Table 5.3. Figure 5.3 shows the DAQ system.

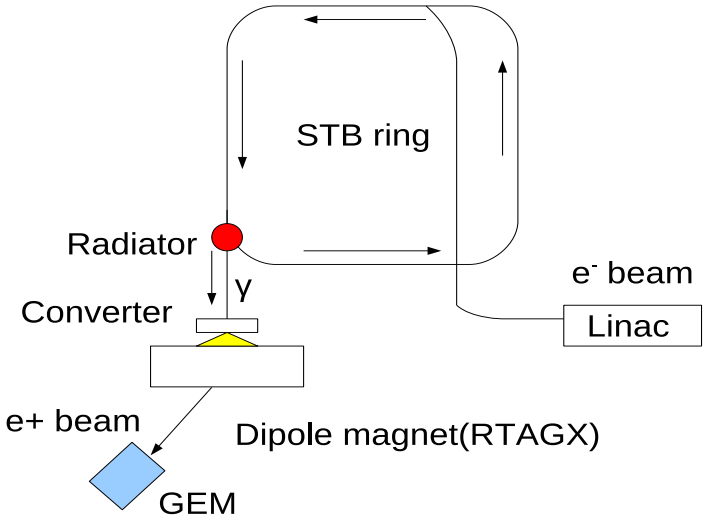

Figure 5.2: A schematic view of the beamline.

Table 5.2: Beam property

particle	momentum	rate	spill	duty factor
e^+	1.0 GeV/c	$\sim$ 4kHz	8 sec	0.58

Table 5.3: The used modules.

module	name	channels	detector
Interrupt register	RPV-130	-	-
Charge sense ADC	V792	32	each scintillator
Peak sense ADC	V785	32	GEM tracker (foil)
TDC	V775	32	GEM tracker, each scintillator
ADC (multiplexed)	V550	2	SSDs
Sequencer	V551B	2	SSDs
Flash ADC	RPV-160	8	GEM tracker (foil)
APVDAQ	APVDAQ	4	GEM tracker (strip)

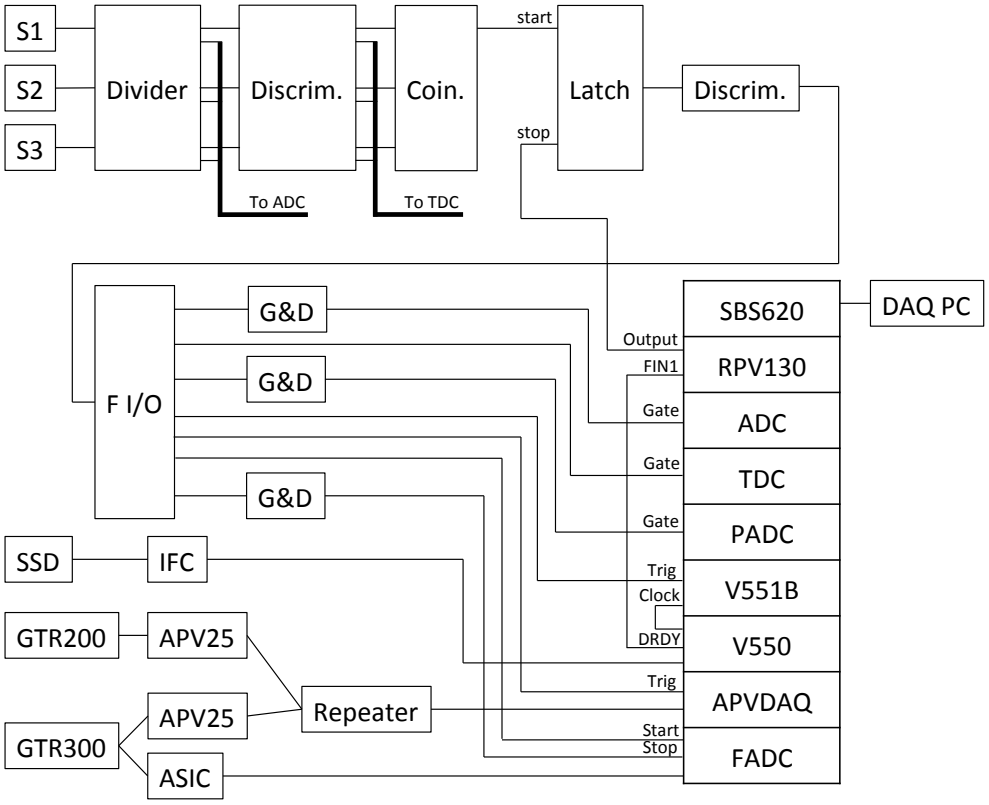

Figure 5.3: The DAQ system.

5.2 Analysis

5.2.1 SSD Analysis

Offset and common mode noise subtraction

A pedestal and common mode noise of ADC need to be subtracted by using pedestal run data. The pedestal run is carried out by clock trigger without beam and its data has ADC value of $384 \times 3 = 1152$ ch. The common mode noise of each VA-chip is also evaluated and subtracted event by event.

First, the common mode noise is evaluated before pedestal evaluation because the common mode noise changes event by event. The common mode noise is caused in every 128 ch due to a characteristic of VA-chip. One SSD has three VA-chips. Therefore, the common mode noise $n_i\,(i = 1, 2, \cdots, 9)$ can be calculated event by event as following.

$$n_i = \sum_{j=1}^{128} \frac{A_{ij}}{128} \tag{5.1}$$

where A_{ij} is ADC value of j th strip in i th VA-chip.

Second, to evaluate pedestal value of each strip ch, the common mode noise is subtracted from ADC value of each strip ch and then the subtracted ADC value is taken the average of whole events. The pedestal mean value of i th strip P_i is given by

$$P_i = \sum_{k=1}^{N_{evt}} \frac{A_{i,k} - n_{j,k}}{N_{evt}} \tag{5.2}$$

where N_{evt} is the number of events, k is a suffix of event number , $A_{i,k}$ is ADC value of i th strip and j is the VA-chip number corresponding to i th strip. The result of evaluation of pedestal value is shown in Fig. 5.4. In addition the pedestal mean value, each standard deviation of the pedestal σ_i is calculated as follow.

$$\sigma^2 = \sum_{k=1}^{N_{evt}} \frac{(A_{i,k} - n_{j,k} - P_i)^2}{N_{evt}} \tag{5.3}$$

Figure 5.5 shows the result of the calculation. There is some dead strips, but these do not mostly have influence on tracking precision since a strip pitch of SSD is sufficiently narrower than that of a GEM tracker.

Finally, in a beam run, the common mode noise is evaluated the same as Eq. (5.1) event by event and corrected ADC value of i th strip a_i is given by

$$a_i = A_i - n_j - P_i \tag{5.4}$$

and, a_i is normalized to significance s_i as following for analysis of a hit position of SSDs.

$$s_i = \frac{a_i}{\sigma_i} \tag{5.5}$$

When a SSD has hit strip on i th strip, the s_i has larger value than the others as shown in Fig. 5.6.

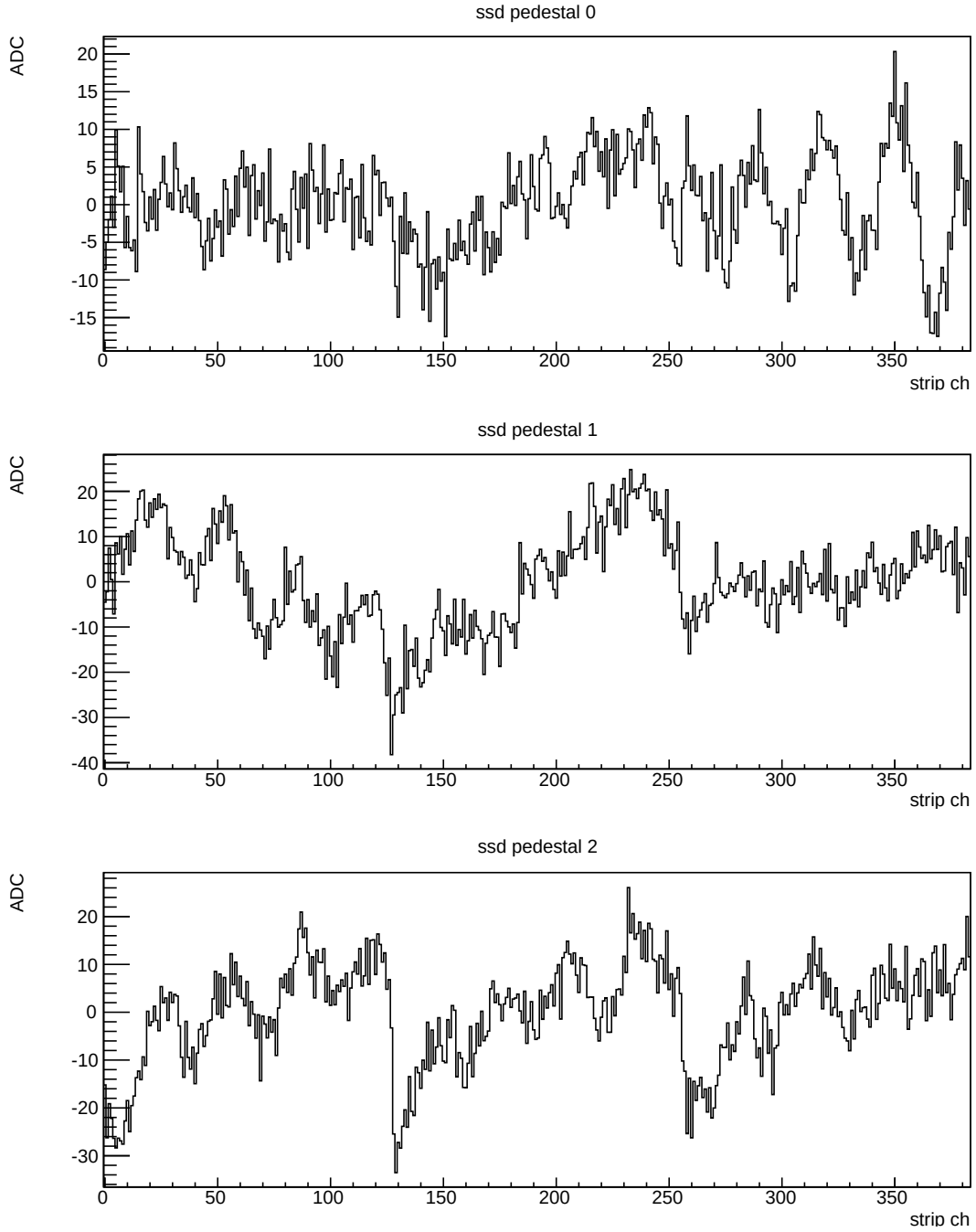

Figure 5.4: The pedestal mean value of SSDs.

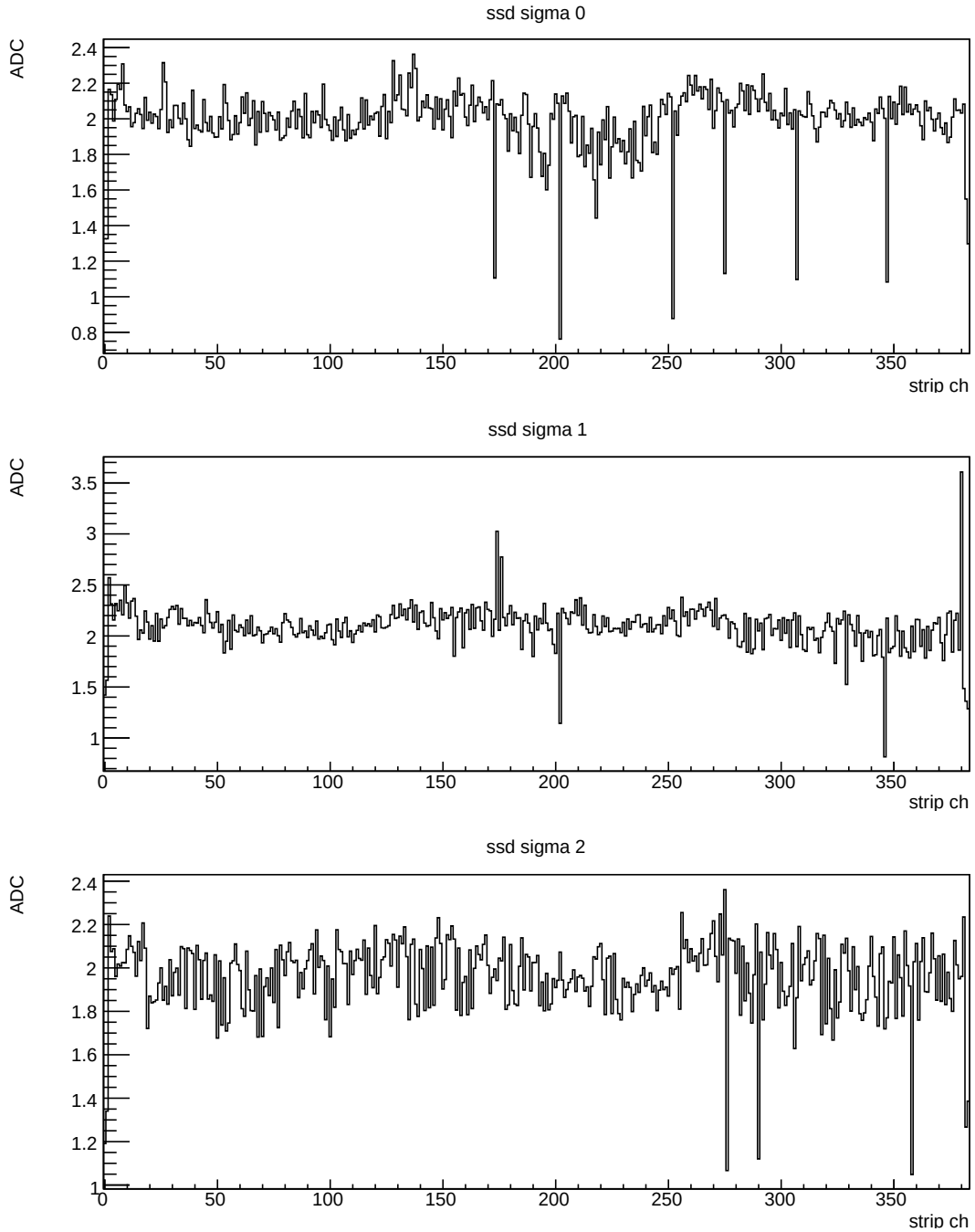

Figure 5.5: The standard deviation of pedestal mean.

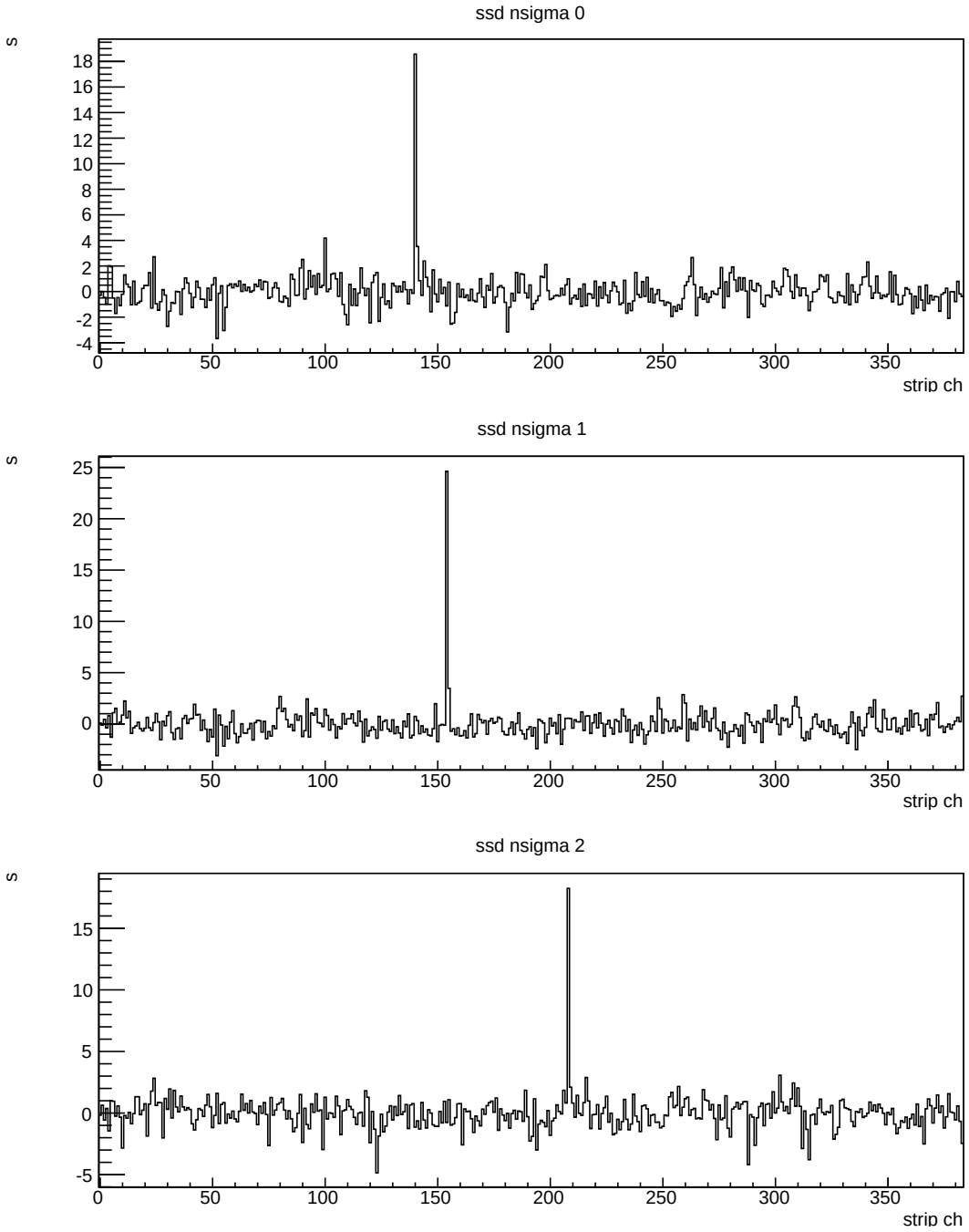

Figure 5.6: An event display of SSD hits. The spike is a hit strip.

Determination of a SSD threshold

A threshold of each SSD is determined in order to define hit strips to calculate a hit position of a track properly. The distribution of the significance is shown in Fig. 5.7, Fig. 5.8 and Fig. 5.9. The distribution of s_i for events of the pedestal is in a range of $2 \sim 8$. The threshold is set to suppress noise hits properly.

Calculation of a SSD hit position

In local coordinates system of each SSD, its hit position $X_{\mathrm{s},i}\,(i = 0, 1, 2)$ is calculated by weighted mean method (also called Center-Of-Gravity (COG) method) as following,

$$X_{\mathrm{s},i} = \frac{0.08\,(\mathrm{mm}) \times \sum_{k=1}^{n_{\mathrm{hit}}} N_k \times s_{N_k}}{\sum_{k=1}^{n_{\mathrm{hit}}} s_{N_k}} \tag{5.6}$$

where $0.08\,(\mathrm{mm})$ is a strip pitch of a SSD, n_{hit} is the number of hit strips, N_k is a hit strip number and s_{N_k} is the significance of N_k.

Event selection

Event selection about information of SSD hits is done to cut invalid events for further analysis.

- Requirement of hits for SSD pairs, such as (SSD0, SSD1) and (SSD1, SSD2).

  To obtain a reference hit position on the $200 \times 200\,\mathrm{mm}^2$ GEM tracker, both a condition that SSD0 has at least one hit strip and the same for SSD1 are required. As the same way, the condition for SSD1 and SSD2 pair is required in order to obtain a reference on the $300 \times 300\,\mathrm{mm}^2$ one.

- Exclusion of double track events.

  Clustering method is applied to hit strips of each SSD in order to count the number of tracks in an event. The clustering is a method of grouping hit strips originated from the same track. In the clustering method, the hit strips are clustered within 1 strip. After the clustering, if the number of tracks equals to 1, then the hit position is calculated by Eq (5.6). Figure 5.10 shows the distribution of the number of tracks in a beam run.

After the event election, approximately 90% of all events in a beam run survives.

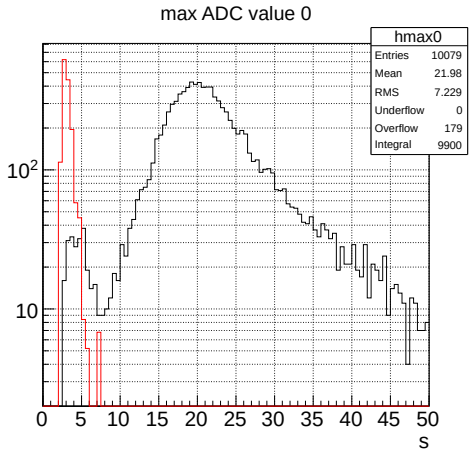

Figure 5.7: Threshold search ssd 0 (Black: Beam run, Red: Pedestal run)

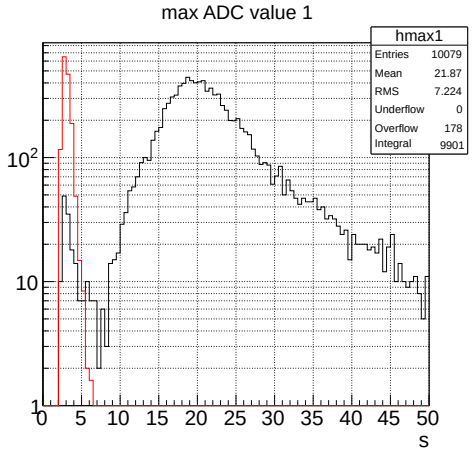

Figure 5.8: Threshold search ssd 1

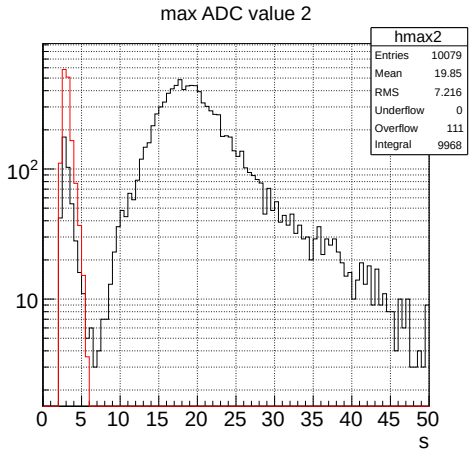

Figure 5.9: Threshold search ssd 2

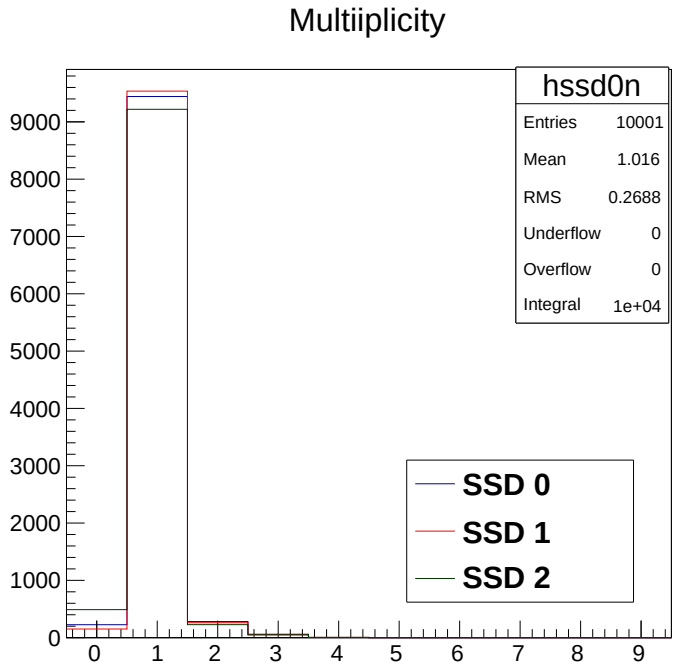

Figure 5.10: The distribution of the number of tracks. Events in which the number of them equals to 1 are selected for further analysis.

Calculation of a reference hit position on GEM trackers

A reference track is determined by a hit position of a SSD and that of the next SSD. Local coordinates of the hit position on the SSDs are converted to the global coordinates which are defined as Fig. 5.1 by using geometrical information. The coordinates of the hit position on the first SSD and the second is defined as a vector $\boldsymbol{x}_1$ and $\boldsymbol{x}_2$ respectively. Then, assuming that the track is a straight line, the line l is given by following equation,

$$l : \boldsymbol{x} = \boldsymbol{x}_1 + t(\boldsymbol{x}_2 - \boldsymbol{x}_1) \tag{5.7}$$

where t is a parameter. A GEM plane S_{gem} can be defined as following equation,

$$S_{\mathrm{gem}} : \boldsymbol{n} \cdot (\boldsymbol{x} - \boldsymbol{x}_{\mathrm{gem}}) = 0 \tag{5.8}$$

where $\boldsymbol{n}$ is the normal vector of the GEM plane and $\boldsymbol{x}_{\mathrm{gem}}$ is an arbitrary vector on the GEM plane. Variables of the plane are determined by geometrical information of the tracker. The reference hit position on the GEM plane $\boldsymbol{x}_{\mathrm{ref}}$ is calculated as the intersection point of l and S_{gem}. Thus, the reference $\boldsymbol{x}_{\mathrm{ref}}$ is given by

$$\boldsymbol{x}_{\mathrm{ref}} = \boldsymbol{x}_1 + \frac{\boldsymbol{n} \cdot (\boldsymbol{x}_{\mathrm{gem}} - \boldsymbol{x}_1)}{\boldsymbol{n} \cdot (\boldsymbol{x}_2 - \boldsymbol{x}_1)} \tag{5.9}$$

In this test experiment, information of y-coordinate is not acquired since the SSD is able to obtain information of only one coordinate. However, without data of y-coordinate, the x and z coordinates of the reference can be determined uniquely

because the y-component of the normal vector is negligible small in the setup of GEM trackers. For after analysis, $X_{\rm ref}$ is defined as the x-component of $\boldsymbol{x}_{\rm ref}$ in the global coordinates system.

5.2.2 GEM tracker Analysis

Pedestal evaluation and subtraction

A pedestal value as a global offset value needs to be evaluated for each strip channel and clock. by using a pedestal run. Before evaluation of the pedestal, common mode noise should be subtracted. A hybrid board of APV25 chips has 6 connectors. There is common mode noise in each connector, and the noise level is different at clock by clock.

The common mode noise of the k-th connector in the j-th clock N_{kj} for an event is evaluated by

$$N_{kj} = \frac{1}{n_k} \sum_{i \in k\text{-th connector}} A_{ij} \tag{5.10}$$

where n_k is the number of channels which the k-th connector has and A_{ij} is a obtained flash ADC value of i-th strip and j-th sampling clock of a APV25 chip. Then, the pedestal value P_{ij} is calculated as following,

$$P_{ij} = \frac{1}{N_{evt}} \sum_{\text{all events}} (A_{ij} - N_{kj}) \tag{5.11}$$

where A_{ij} and N_{kj} is calculated event by event, N_{evt} is the number of total events in a pedestal run. Therefore, a corrected flash ADC value A^c_{ij} in an event is obtained by

$$A^c_{ij} = (A_{ij} - N_{kj}) - P_{ij} \tag{5.12}$$

Figure 5.11 shows a typical shape of A^c_{ij}.

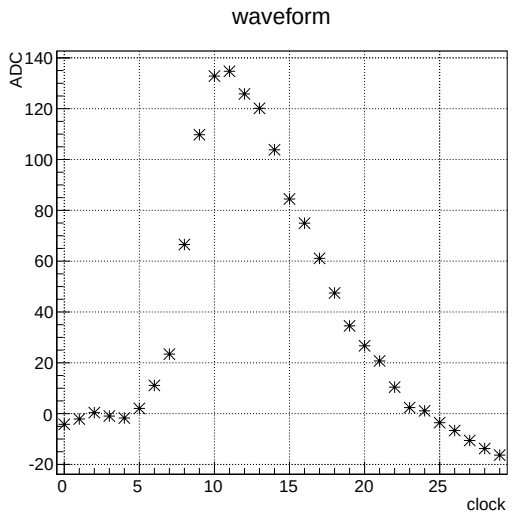

Figure 5.11: A typical shape of corrected ADC A^c_{ij}

Plotting all A_{ij}^{c} makes an event display as shown in Fig. 5.12, Fig. 5.13 and Fig. 5.14.

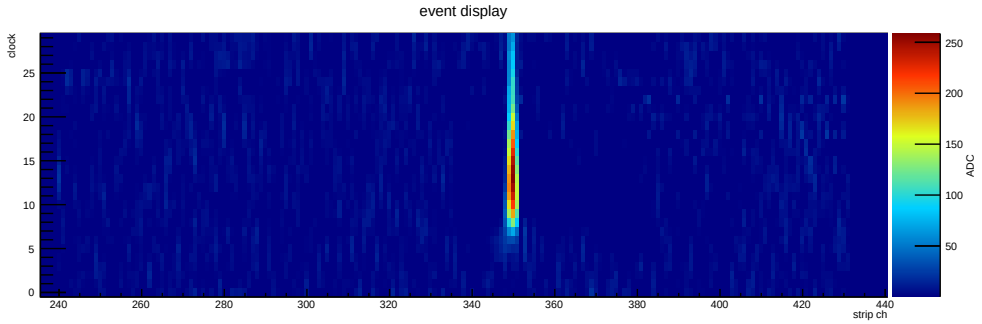

Figure 5.12: event display: GTR 300 x-strip 0°, The horizontal axis is the strip channel number, the vertical axis is the sampling clock number and the color means ADC value.

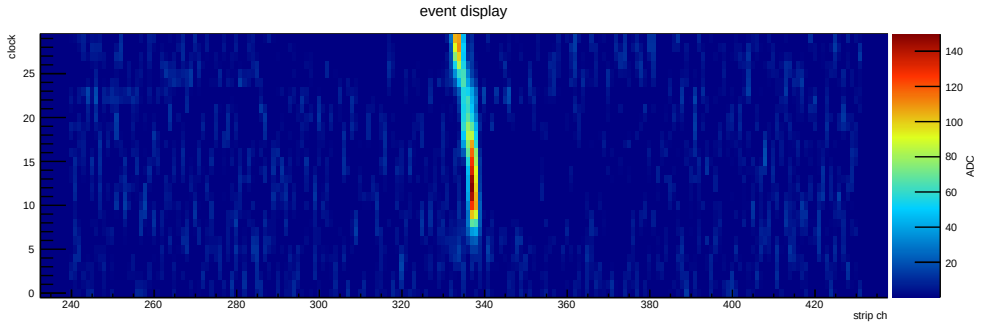

Figure 5.13: event display: GTR 300 x-strip 15°

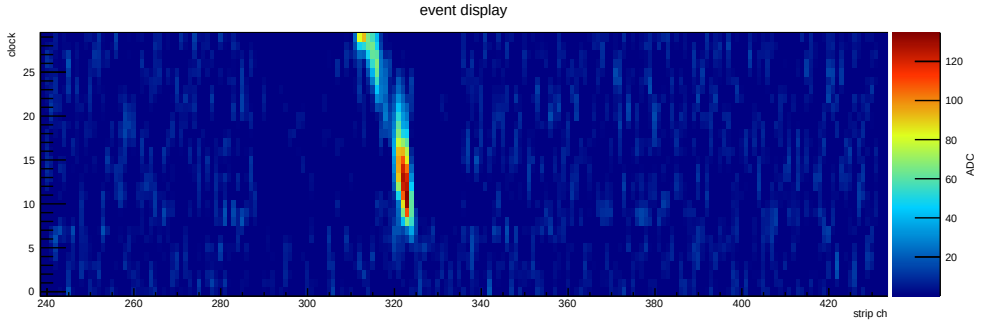

Figure 5.14: event display: GTR 300 x-strip 30°

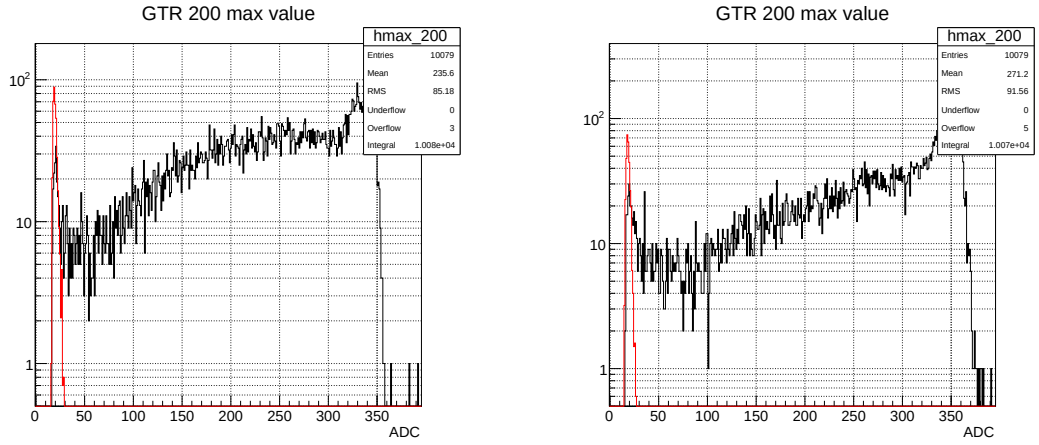

Figure 5.15: Threshold search of the $200 \times 200\,\mathrm{mm}^2$ GEM tracker (left: X strip, right: Y strip)

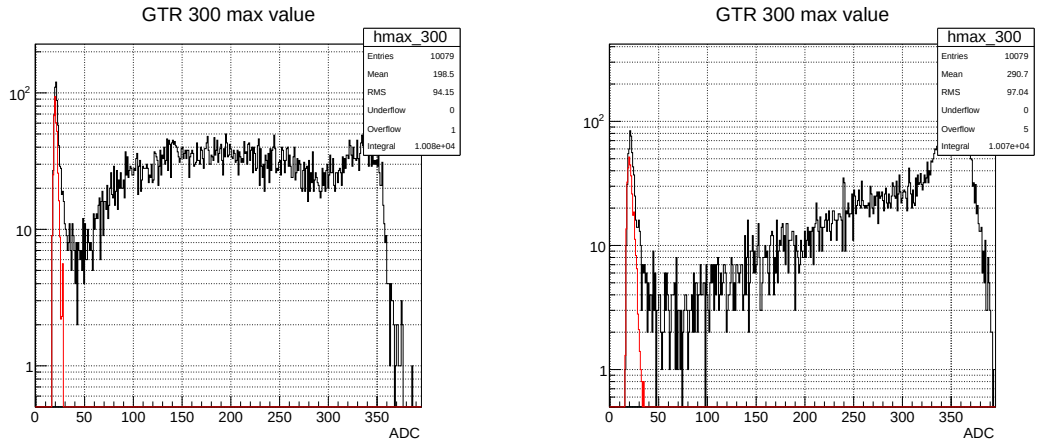

Figure 5.16: Threshold search of the $300 \times 300\,\mathrm{mm}^2$ GEM tracker (left: X strip, right: Y strip)

Determination of threshold for GEM trackers

As the same way of SSDs, a threshold is set to cut noise hits properly. The distribution of the maximum value of A_{ij} for events and a pedestal is shown in Fig. 5.15 and Fig. 5.16. The red line is the distribution of the pedestal and the black one is that of events. The threshold value is set to 30 for all strips.

Searching hit strips and clustering

Charge of the i-th strip Q_i is defined as the peak value of the waveform of A^c_{ij}. If Q_i exceeds the threshold, the i-th strip is regard as a member of "hit strips". Ionized electrons by a track spread over several strips due to a diffusion in an electron drift and injection angle of the original track. Therefore the hit strips which originate from the same track should be grouped. This group is called a cluster. Clustering means a method to make a cluster. We search the hit strips for all the strips and

then do clustering. Clustering condition for the hit strips is defined as follow

$$h_{i+1} - h_i \leq n \quad (i = 1, 2, \cdots, N-1; n = 1, 2, \cdots) \tag{5.13}$$

where h_i is the strip number of the i-th hit, N is the number of the hit strips and n is a parameter. Note an angled track can produce discontinuity hits and the parameter n is optimized for the analysis. Each cluster has one hit position. The hit position is calculated by the cluster information, such as the charge Q_i and arrival times of hits in the cluster.

Calculation of a hit position for each cluster

A hit position of a GEM tracker is calculated on the plane which is the center of drift gap. X_{gem} is defined as a hit positions in local coordinates system of a GEM tracker. There is two method to calculate X_{gem} from a cluster.

Center-Of-Gravity (COG) method

X_{gem} is calculated by the same way of Eq (5.6),

$$X_{\text{gem}} = \frac{0.35\,(\text{mm}) \times \sum_{k=1}^{n_{\text{cl}}} h_k \times Q_{h_k}}{\sum_{k=1}^{n_{\text{cl}}} Q_{h_k}} \tag{5.14}$$

where n_{cl} is the number of hit strips in a cluster. The strip pitch is 0.35 mm. This method is applied for tracks whose incident angle is zero.

Timing fit method

Positions where ionized electrons is generated in the drift gap are reconstructed by using timing information of hits and drift velocity v_d. Arrival time of hits at the readout is defined as the APV25 clock number at which the signal A^c_{ij} exceeds half of the peak value of the waveform as shown in Fig. 5.17. Difference of the arrival time among the hit strips in the cluster corresponds to difference of the points where electrons ionized (ionization point). Then, the relation between the hit strip number and the arrival time is applied to a linear fit as shown in Fig. 5.18. To convert fit parameters to track information, the variables are scaled as following,

$$x = (\text{strip number}) \times 0.35\,(\text{mm}), \quad z = v_d \times (\text{APV clock}) \times 25\,\text{ns} \tag{5.15}$$

where v_d is drift velocity and 25 ns is a sampling clock of APV25. The drift velocity v_d is estimated empirically by using the inclination of the fit function a_0 and the incident angle θ.

$$v_d\,(\text{cm}/\mu\text{s}) = \frac{0.035\,(\text{cm}) \times \tan(90^\circ - \theta)}{0.025\,(\mu\text{s}) \times a_0} \tag{5.16}$$

An example of the distribution of the drift velocity is shown in Fig. 5.19. After the scaling, the track is obtained as $z = ax + b$. Therefore, X_{gem} is calculated by

$$X_{\text{gem}} = \frac{z_{\text{center}} - b}{a} \tag{5.17}$$

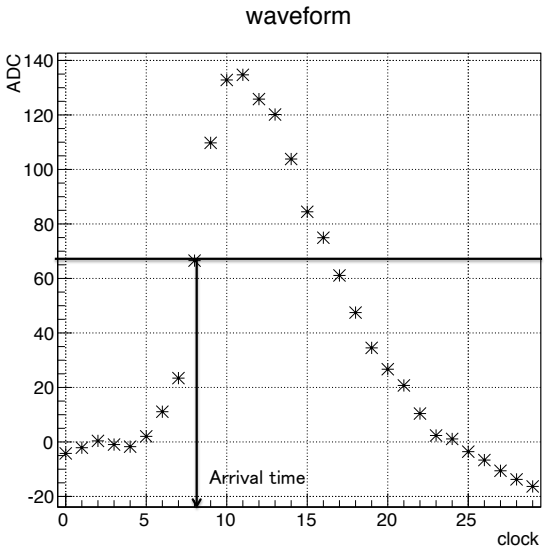

Figure 5.17: Arrival time

where z_{center} is the z-coordinate of the center of drift plane.

When the number of hit strips in a cluster is less than 4, the precision of the fitting is not good enough. In this situation, X_{gem} is calculated by

$$X_{\text{gem}} = 0.035\,(\text{mm}) \times \frac{1}{2}(h_1 + h_{n_{cl}}) \tag{5.18}$$

where n_{cl} is the number of hit strips in the cluster.

Additional cut

The $200 \times 200\,\text{mm}^2$ GEM tracker has a insensitive region as shown in Fig. 5.20. The histogram shows hit counts of each strip in a beam run. The insensitive region ranges from the 286-th channel to the 290-th. This range corresponds to a dead region of $0.35 \times 5 = 1.75\,\text{mm}$. In order to evaluate a position resolution and efficiency on active region, we cut events in which the reference hit position determined by SSDs is within the region.

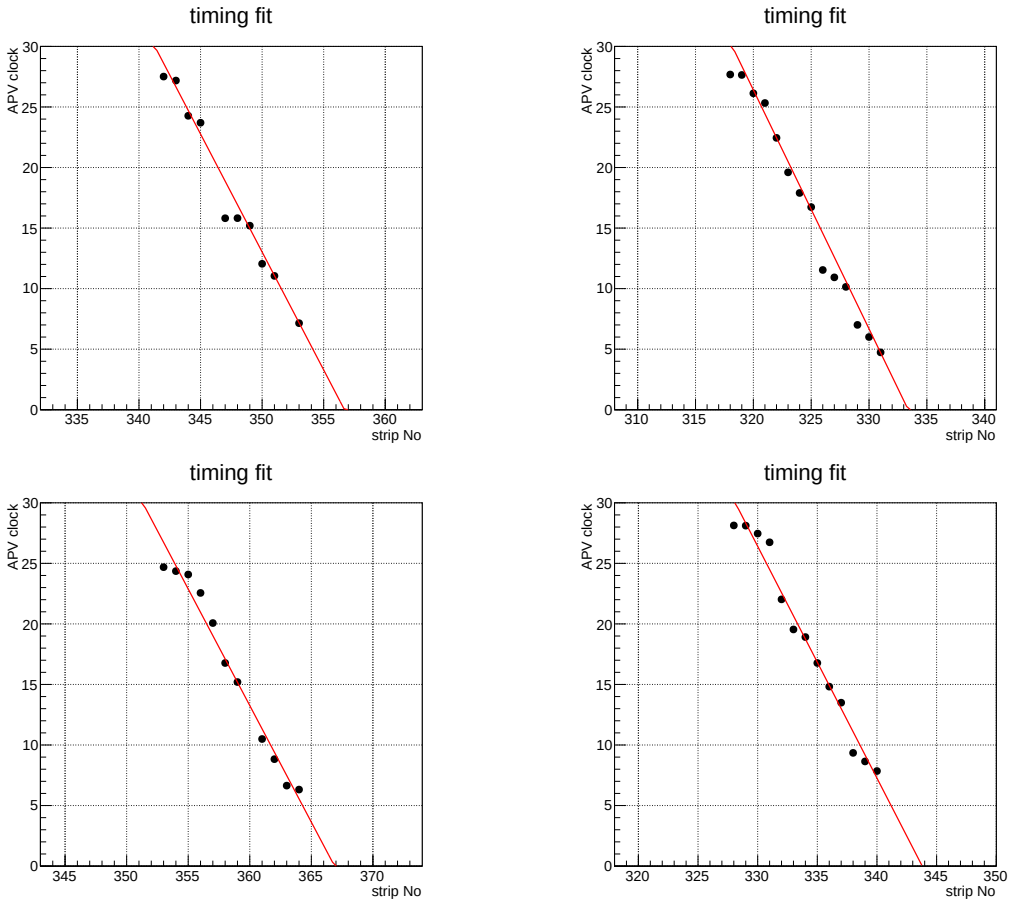

Figure 5.18: Display of timing fit method (incident angle is 30°)

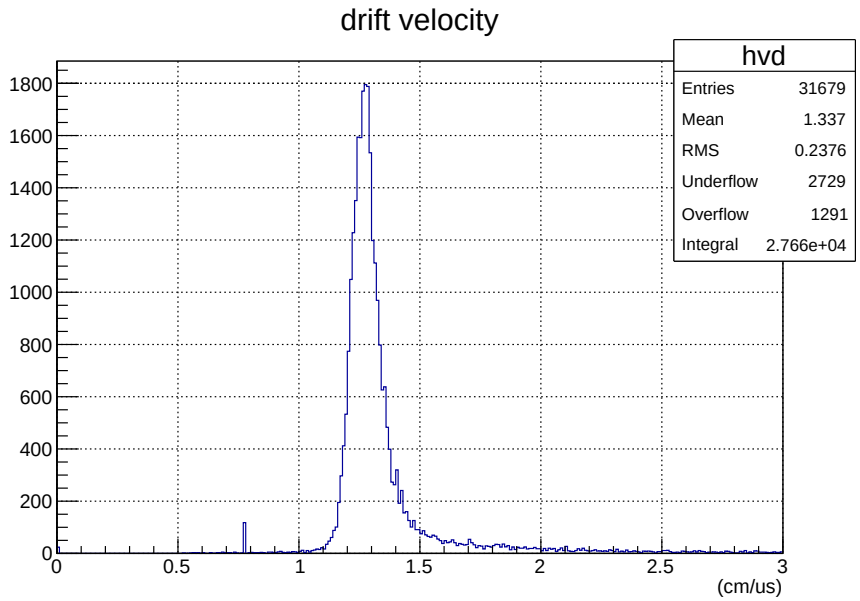

Figure 5.19: The distribution of drift velocity

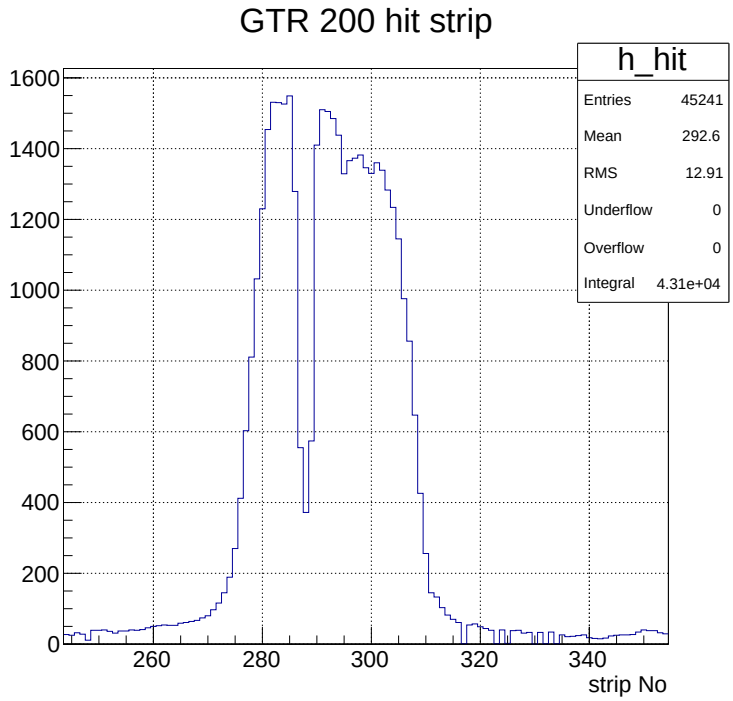

Figure 5.20: An insensitive region of the $200 \times 200\,\mathrm{mm}^2$ GEM tracker.

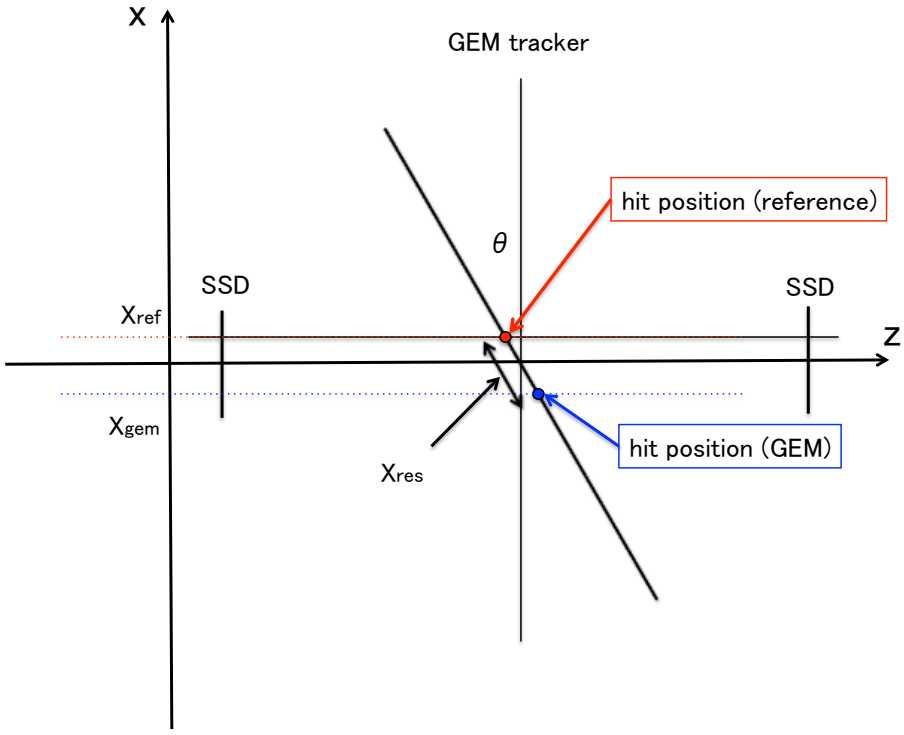

Figure 5.21: Geometry for hit positions of SSDs and a GEM tracker.

Residual distribution

A residual distribution is made by a subtraction of GEM hit position from the estimated hit position by each SSD. The residual X_{res} is calculated as following,

$$X_{\mathrm{res}} = \frac{X_{\mathrm{gem}} - X_{\mathrm{ref}}}{\cos\theta} \tag{5.19}$$

where X_{gem} and X_{ref} are the x-component of a hit position determined by the GEM tracker and a reference hit positron determined by SSDs, respectively, in the global coordinates system and, θ is the incident angle determined by the setup as shown in Fig. 5.21. The obtained residual distribution is shown in Fig. 5.22 - Fig. 5.27. The residual distribution is fitted by a Gaussian function and resolutions of position measurements by GEM is evaluated as a sigma of the fitted function.

Evaluation of efficiency

The efficiency of the GEM tracker ϵ is defined as following.

$$\epsilon = \frac{N_{\mathrm{eff}}}{N_{\mathrm{tot}}} \tag{5.20}$$

where N_{tot} is the number of total events in which a reference track can be determined by SSDs and N_{eff} is the number of efficient events. In case of the $200 \times 200\,\mathrm{mm}^2$ GEM tracker, the number of events in which the reference hit position is in the dead

region of the tracker is subtracted from $N_{\rm tot}$. $N_{\rm eff}$ is defined as the number of events satisfying the following condition

$$|X_{\rm res}| < 1\,{\rm mm} \tag{5.21}$$

Effect of multiple scattering

To evaluate a position resolution of the GEM trackers from the residual sigma, effect of multiple scattering needs to be estimated. We define the position resolution of the GEM tracker and that of SSDs as $\sigma_{\rm gem}$ and $\sigma_{\rm SSD}(= 80/\sqrt{12}\,\mu{\rm m})$, respectively. The x-coordinates on which a positron truly hits are defined as R_0, R_1 and R_2 from the upper stream of the beam as shown in Fig. 5.28. Note R_i is not a position detected by each detector. Assuming the positron transports in vacuum, the x-coordinates of hit positions are defined as V_0, V_1 and V_2 from the upper stream. Thus, R_i is a position where V_i is effected by multiple scattering. Effect of multiple scattering between SSD1 and a tracker is defined as ms_1 and that between the tracker and SSD2 is defined as ms_2.

$$R_1 = V_1 + ms_1$$
$$R_2 = V_2 + ms_1 + ms_2$$

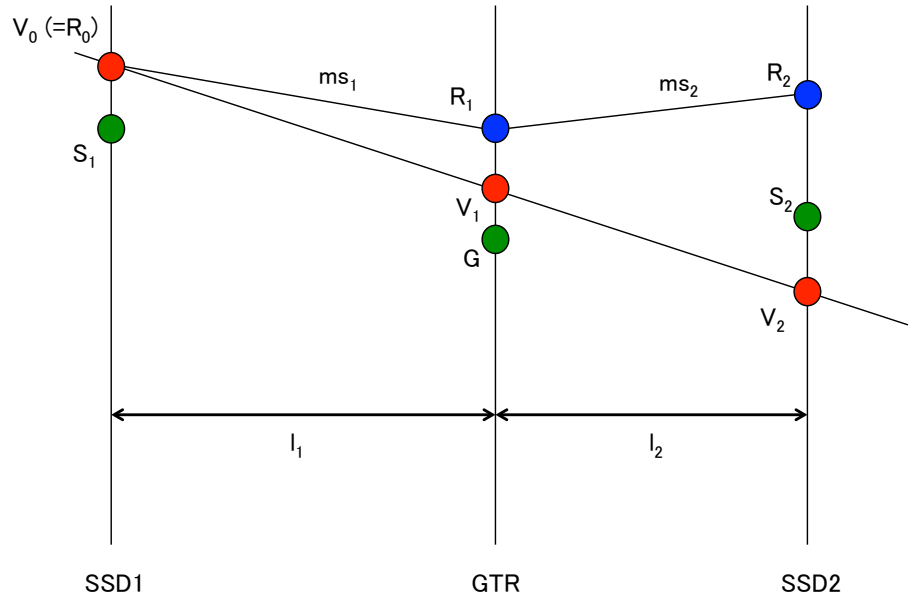

Figure 5.28: Geometry for evaluation of multiple scattering effect.

Hit positions actually detected by the SSDs are defined as S_1 and S_2, and a hit position detected by the GEM tracker is defined as G. S_1,S_2 and $G(= X_{\rm gem})$ are given by

$$S_1 = R_0 + \sigma_{\rm SSD} = V_0 + \sigma_{\rm SSD}$$
$$S_2 = R_2 + \sigma_{\rm SSD} = V_2 + ms_1 + ms_2 + \sigma_{\rm SSD}$$
$$G = R_1 + \sigma_{\rm gem} = V_1 + ms_1 + \sigma_{\rm gem}$$

The reference hit positron X_{ref} is given by linear interpolation

$$\begin{aligned} X_{\text{ref}} &= \frac{l_2}{L} S_1 + \frac{l_1}{L} S_2 \\ &= V_1 + \sigma_{\text{SSD}} + \frac{l_1}{L}(ms_1 + ms_2) \end{aligned}$$

Then, the residual r is calculated by

$$r = G - X_{\text{ref}} = \sigma_{\text{gem}} - \sigma_{\text{SSD}} + \frac{l_2}{L} ms_1 - \frac{l_1}{L} ms_2 \tag{5.22}$$

Therefore, σ_{gem} is evaluated by following.

$$\begin{aligned} \sigma_{\text{gem}} &= \sqrt{\sigma_{\text{res}}^2 - \sigma_{\text{SSD}}^2 - \sigma_{\text{MS}}^2} \\ \sigma_{\text{MS}} &= \sqrt{\left(\frac{l_2}{L} ms_1\right)^2 + \left(\frac{l_1}{L} ms_2\right)^2} \end{aligned}$$

where σ_{res} is the residual sigma and σ_{MS} is the term for the effect of multiple scattering.

The value of ms_i is calculated as following.

$$ms_i = \frac{l_i}{\sqrt{3}} \times \frac{13.6\,\text{MeV}}{\beta cp} \sqrt{l_{\text{rad}}}\,[1 + 0.038 \ln(l_{\text{rad}})] \tag{5.23}$$

where p is momentum of the beam and $l_{\text{rad}} (\sim x/X_0)$ is normalized radiation length in l_i. The radiation length l_{rad} can be calculated by material budget of the GEM trackers and of air, and geometry information. We can convert the residual sigma to the position resolution as following.

$$\sigma_{\text{gem}} = \begin{cases} \sqrt{\sigma_{\text{res}}^2 - 23^2 - 16^2} & (200 \times 200\ \text{mm}^2\ \text{GEM tracker}) \\ \sqrt{\sigma_{\text{res}}^2 - 23^2 - 21^2} & (300 \times 300\ \text{mm}^2\ \text{GEM tracker}) \end{cases} \tag{5.24}$$

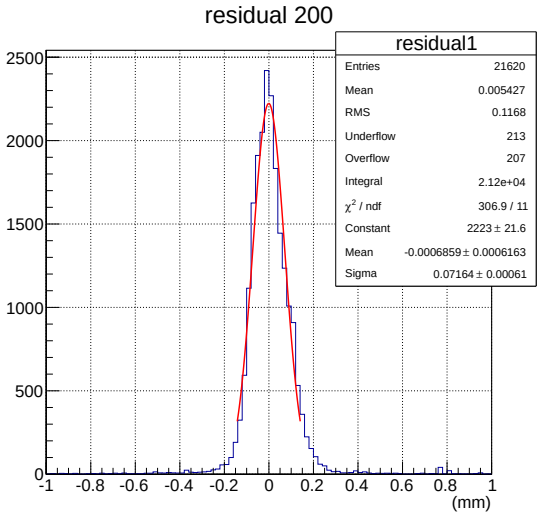

Figure 5.22: GTR200: incident angle 0°

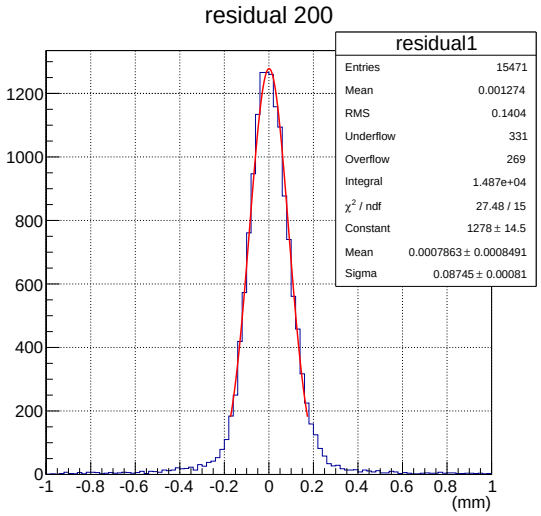

Figure 5.23: GTR200: incident angle 15°

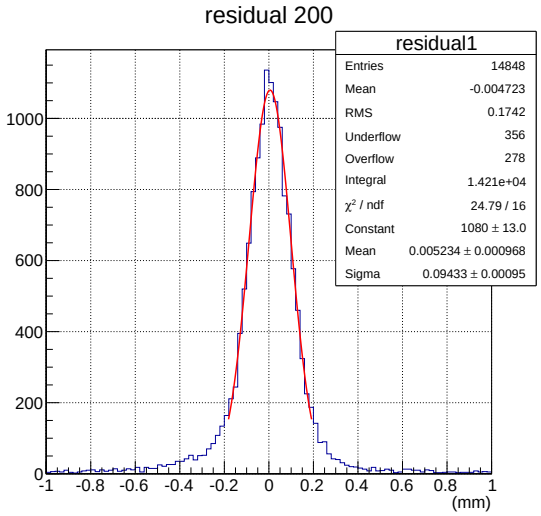

Figure 5.24: GTR200: incident angle 30°

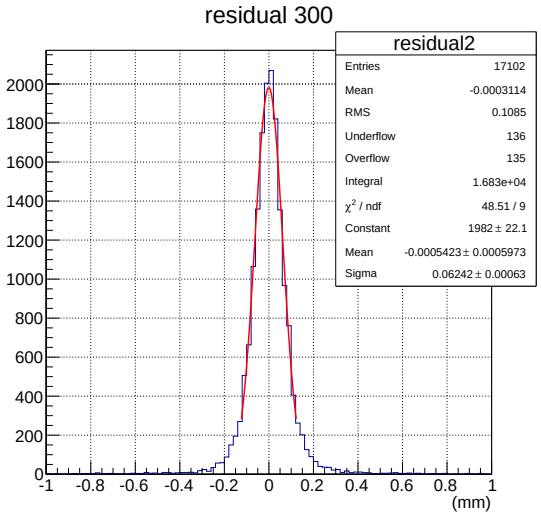

Figure 5.25: GTR300: incident angle 0°

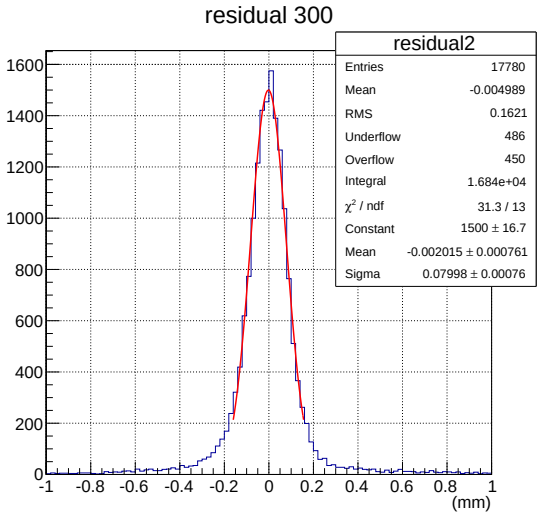

Figure 5.26: GTR300: incident angle 15°

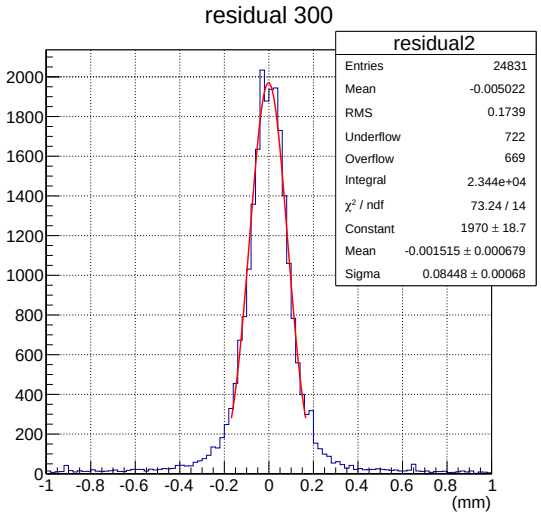

Figure 5.27: GTR300: incident angle 30°

5.3 Result

The obtained position resolutions for two sizes of the GEM trackers as a function of the incident angle are shown in Fig. 5.29. The position resolution of both the $200 \times 200\,\mathrm{mm}^2$ and $300 \times 300\,\mathrm{mm}^2$ is better than required resolution ($100\,\mu\mathrm{m}$) for the incident angle from 0° to 30°. This result satisfies our requirement.

The obtained efficiency for two sizes of GEM trackers as a function of the incident angle are shown in Fig. 5.30. The $200 \times 200\,\mathrm{mm}^2$ tracker is achieved high detection efficiency of $94 \sim 97\%$. The efficiency of the $300 \times 300\,\mathrm{mm}^2$ tracker is relatively low detection of $88 \sim 93\%$.

The test setups is summarized in Table 5.4.

Table 5.4: The test setups.

GEM size (mm)	strip pitch (μm)	drift gap (mm)	V_{GEM}	drift field (V/cm)	angle ($^\circ$)
200	350	6	395	1000	0
200	350	6	395	1000	15
200	350	6	395	1000	30
300	350	6	375	1000	0
300	350	6	375	1000	15
300	350	6	375	1000	30

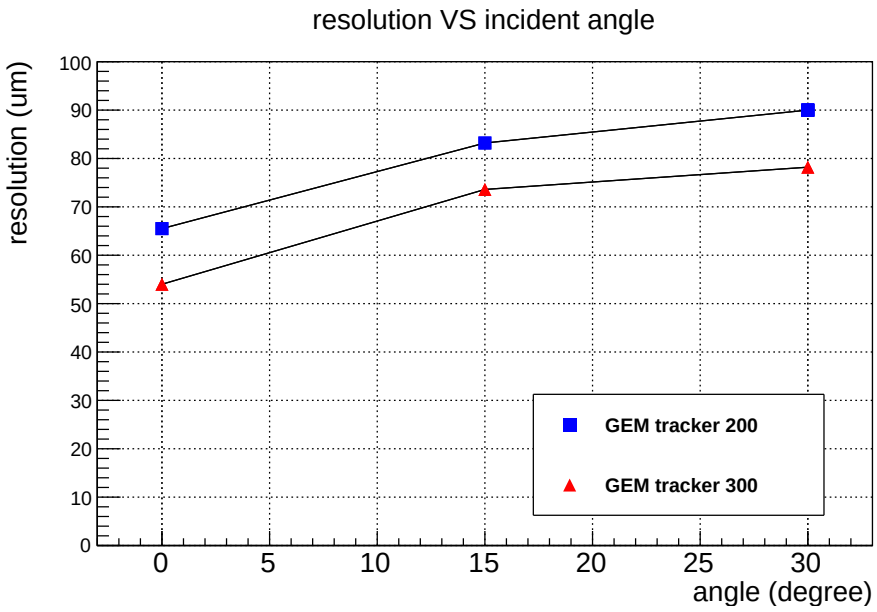

Figure 5.29: Resolution vs angle.

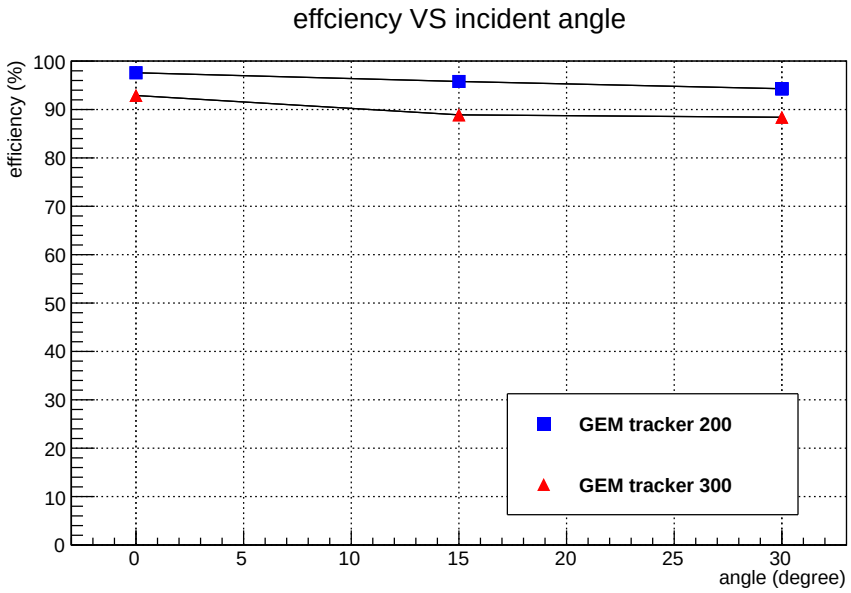

Figure 5.30: Efficiency vs angle

Chapter 6

Conclusion

In the J-PARC E16 experiment, mass spectra of light vector mesons in nuclear matter are measured with high precision and high statistics to investigate a restoration of the chiral symmetry at a normal nuclear density. The mass spectra is measured using electron positron decays to avoid a final state interaction.

For the E16 experiment, a new spectrometer which has high rate capability for high intensity beam at J-PARC and a good mass resolution is need to be constructed. The spectrometer consists of trackers for momentum measurements and electron identification counters. A GEM tracker is used for tracking charged particles. The GEM tracker is required to have a good spatial resolution better than 100 μm for an incident angle from 0° to 30°. Three sizes of GEM trackers, such as $100 \times 100, 200 \times 200$ and $300 \times 300\,\mathrm{mm}^2$, are necessary to cover a large acceptance. The $300 \times 300\,\mathrm{mm}^2$ GEM tracker needs to generate a trigger signal from the last GEM foil. A large GEM tracker was developed to fulfill the requirements.

Development of trigger signal generation from a GEM foil was succeeded using a discrete preamplifier and an existing ASIC. Characteristics of the trigger signal and noise levels are evaluated. A new prototype of a GEM trigger system was constructed using obtained information. For the new trigger system, a new GEM foil which has 24 electrodes and a new dedicated ASIC are developed and their performance are evaluated. As a result, the new developed large GEM has gain of 10^4 which enough to achieve a good spatial resolution and high trigger efficiency, The new ASIC can successfully pick a trigger signal from GEM foil.

The position resolution and the efficiency of the large GEM trackers are evaluated using a beam whether their performance can satisfy our requirement or not. The obtained position resolution is better than 100 μm for the incident angle from 0° to 30°.

As a conclusion, we are ready to start a final detector production for the GEM trackers.

Acknowledgments

I would like to appreciate Prof. K. Ozawa for his patient support and kind advices. I also express my gratitude to Prof. H. Enyo, Dr. M. Sekimoto, Dr. S. Yokkaichi for their great advices. I would like to thank Dr. K. Aoki, Dr. Y. Aramaki, Dr. Y. Morino, Dr. T. Takahashi, and Dr. D. Kawama for their kindness and great support.

I also thank Dr. T. Ishikawa and Tohoku ELPH group who enable us to use beam for the test experiment. I express my gratitude Prof. M. Tanaka and Open-It whose help was indispensable to develop the ASIC.

I would like to appreciate Mr. Y. Komatsu for his great support and advices. I express my thank to Mr. W. Nakai for his great advices and construction of DAQ system. I also thank Mr. Y. Watanabe, Mr. K. Kanno, Mr. S. Masumoto, Mr. T. Adachi, Mr. T. Shibukawa and Ms. H. Murakami for great advices in meetings.

Bibliography

[1] D. J. Gross and F. Wilczek, Phys. Rev. Lett. **30**, 1343 (1973).

[2] J. Beringer *et al.*, Phys. Rev. D **86**, 010001 (2012).

[3] K. G. Wilson, Phys. Rev. D **10**, 2445 (1974).

[4] Y. Nambu and G. Jona-Lasinio, Phys. Rev. **122**, 345 (1961).

[5] Y. Nambu and G. Jona-Lasinio, Phys. Rev. **124**, 246 (1961).

[6] W. Weise, Nuclear Physics A **553**, 59 (1993).

[7] G. E. Brown and M. Rho, Phys. Rev. Lett. **66**, 2720 (1991).

[8] T. Hatsuda and S. H. Lee, Phys. Rev. C **46**, R34 (1992).

[9] F. Klingl, N. Kaiser, and W. Weise, Nuclear Physics A **624**, 527 (1997).

[10] J. I. Kapusta and E. V. Shuryak, Phys. Rev. D **49**, 4694 (1994).

[11] E. Drukarev and E. Levin, Progress in Particle and Nuclear Physics **27**, 77 (1991).

[12] D. Adamov *et al.*, Physics Letters B **666**, 425 (2008).

[13] S. Damjanovic, Nuclear Physics A **783**, 327 (2007).

[14] R. Muto *et al.*, Phys. Rev. Lett. **98**, 042501 (2007).

[15] M. Naruki *et al.*, Phys. Rev. Lett. **96**, 092301 (2006).

[16] M. H. Wood *et al.*, Phys. Rev. C **78**, 015201 (2008).

[17] D. Trnka *et al.*, Phys. Rev. Lett. **94**, 192303 (2005).

[18] T. Ishikawa *et al.*, Physics Letters B **608**, 215 (2005).

[19] F. Sauli, Nucl. Instr. and Meth A **386**, 531 (1997).

[20] B. Ketzer, Q. Weitzel, S. Paul, F. Sauli, and L. Ropelewski, Nucl. Instr. and Meth A **535**, 314 (2004).

[21] `http://gdd.web.cern.ch/GDD/`.

[22] M. Raymond *et al.*, in *IEEE NSS Conference Record*, volume 2, pp. 9/113–9/118 vol.2, 2000.

[23] `http://openit.kek.jp`.